ผลกระทบของการรีคริสตัลไลเซชันและการขยายขนาดเกรน

ต่อการเกิดแอนนีลลิงทวินในเหล็กกล้าไร้สนิม 304

นางสาว ปิยะพร ลิ้นโศรก

EFFECTS OF RECRYSTALLIZATION AND GRAIN GROWTH

ON THE FORMATION OF ANNEALING TWIN

IN THE 304 STAINLESS STEEL

MISS PIYAPORN SINSROK

A Thesis Submitted in Partial Fulfillment of the Requirements

for the Degree of Master of Science in Nuclear Technology

Department of Nuclear Technology

Faculty of Engineering

Chulalongkorn University

Academic Year 1999

Thesis Title   Effects of Recrystallization and Grain Growth on the Formation of Annealing Twin in the 304 Stainless Steel

By   Miss Piyaporn Sinsrok

Department   Nuclear Technology

Thesis Advisor   Assist. Prof. Dr. Visit Thaveeprungsriporn

Thesis Co-advisor   Mr. Decho Thong-Aram

Accepted by the Faculty of Engineering, Chulalongkorn University in Partial Fulfillment of the Requirements for the Master 's Degree

.... Dean of Faculty of Engineering

(Professor. Dr. Somsak Panyakeow)

THESIS COMMITTEE

.... Chairman

(Associate Professor Nares Chankow)

.... Thesis Advisor

(Assistant Professor Dr. Visit Thaveeprungsriporn)

.... Thesis Co-advisor

(Mr. Decho Thong-Aram)

.... Member

(Assistant Professor Attaporn Pattarasumunt)

ปิยะพร สิ้นโศรก : ผลกระทบของการรีคริสตัลไลเซชันและการขยายขนาดเกรนต่อการเกิดแอนนีลลิงทวิน ในเหล็กกล้าไร้สนิม 304. (EFFECTS OF RECRYSTALLIZATION AND GRAIN GROWTH ON THE FORMATION OF ANNEALING TWIN IN THE 304 STAINLESS STEEL) อ. ที่ปรึกษา : ผศ.ดร. วิศิษฐ ทวีปรังษีพร , อ. ที่ปรึกษาร่วม : อ. เดโช ทองอร่าม , 79 หน้า. ISBN 974-334-963-4.

วิทยานิพนธ์ฉบับนี้มีวัตถุประสงค์หลักคือ การเพิ่มจำนวนขอบเกรนชนิดมีระเบียบ (Coincidence-site–lattice boundary, CSLB) ในเหล็กกล้าไร้สนิมชนิด 304 เพื่อให้ทนต่อการแตกตามขอบเกรน โดยวิธีให้ความร้อน เชิงกล แบบ Recrystallization, One-step strain annealing และ Iterative strain annealing การวิเคราะห์ชนิด ของขอบเกรนทำได้โดยเทคนิค การกระเจิงของอิเล็กตรอนในกล้องจุลทรรศน์อิเล็กตรอนแบบส่องกราด (Electron Back-scattering diffraction pattern, EBSP) จากการทดลองโดยใช้กระบวนการให้ความร้อนทั้งสามชนิดพบว่า การให้ความร้อนเชิงกล แบบ Recrystallization และ One-step strain annealing ไม่สามารถเพิ่มจำนวน CSLB ให้เพียงพอที่จะทำให้เหล็กกล้าไร้สนิมทนต่อการผุกร่อนตามขอบเกรน ในขณะที่ Iterative strain annealing สามารถเพิ่มจำนวน CSLB ได้มากถึง 54% ในชิ้นงานที่ผ่านกระบวนการรีคริสตัลไลซ์ที่ 850°Cเป็นเวลา 2 ชั่วโมง. หลังจากนั้นให้ความเครียดที่ 3% แล้วนำไปอบให้ความร้อนที่ 950°Cเป็นเวลา 10 นาที ซ้ำกัน3 ครั้ง

ภาควิชา นิวเคลียร์เทคโนโลยี   ลายมือชื่อนิสิต ....ปิยะพร สิ้นโศรก.........

สาขาวิชา นิวเคลียร์เทคโนโลยี   ลายมือชื่ออาจารย์ที่ปรึกษา ....

ปีการศึกษา 2542   ลายมือชื่ออาจารย์ที่ปรึกษาร่วม ....

PIYAPORN SINSROK : EFFECTS OF RECRYSTALLIZATION AND GRAIN GROWTH ON THE FORMATION OF ANNEALING TWIN IN THE 304 STAINLESS STEEL. THESIS ADVISOR : ASSIST.PROF.DR. VISIT THAVEEPRUNGSRIPORN, THESIS COADVISOR : MR. DECHO THONG-ARAM, 79 pp. ISBN 974-334-963-4.

The objective of this thesis was to increase the fraction of structurally ordered boundary (Coincidence-site-lattice boundary, CSLB) in 304 stainless steel in an attempt to improve its intergranular corrosion properties. Methods used to increase the CSLB fraction were based on the thermomechanical processing including recrystallization, one-step strain annealing, and iterative strain annealing. The Electron Back-scattering Diffraction Pattern (EBSP) in scanning electron microscope (SEM) was employed to characterize type and fraction of grain boundaries. The results show that recrystallization and one-step strain annealing processes do not increase the fraction of CSLB sufficiently to resist intergranular corrosion. Meanwhile, iterative strain annealing was found to increase the CSLB fraction up to 54% in the specimen recrystallized at 850°C for 2 hr, then underwent 3 sequential strain annealing steps consisting 3% reduction in thickness and heat treated at 950°C for 10 min.

ภาควิชา นิวเคลียร์เทคโนโลยี   ลายมือชื่อนิสิต ...ปิยะพร สินโรจน์...............

สาขาวิชา นิวเคลียร์เทคโนโลยี   ลายมือชื่ออาจารย์ที่ปรึกษา.........................

ปีการศึกษา 2542   ลายมือชื่ออาจารย์ที่ปรึกษาร่วม ....

Acknowledgements

หน้านี้หายไป ไม่มีในต้นฉบับที่นำมาสแกน

Contents

Contents (cont.)

Contents (cont.)

Table contents

Figure contents

Figure contents (cont.)

Figure contents (cont.)

CHAPTER I

INTRODUCTION

1.1 Background

Stainless steels have been widely used in industries where high temperature and high corrosion resistance are required. In nuclear power plants stainless steels are also extensively used in piping systems and steam generators. However, numerous failure of stainless steels have occurred because of intergranular stress corrosion cracking (IGSCC), figure 1.1. It is well understood that IGSCC occurred by a manifestation of three variables: stress, environment, and susceptible microstructures caused by chromium carbide precipitation at grain boundary leading to grain boundary chromium depletion, figure 1.2.

Efforts to control and minimize IGSCC were developed and the three following methods are usually employed to control and minimize IGSCC in stainless steel [1]: 1) high temperature solution heat treatment by heat treating at 1065-1120°C followed by water quenching to dissolve chromium carbides and homogenize the alloys; 2) adding elements which are strong carbide former such as niobium and titanium resulting in stainless steels of type 347 and type 321, respectively; and 3) lowering the carbon content below 0.03% inhibiting formation of carbides. Realizing the IGSCC susceptibility of 304

stainless steels, boiling water reactors (BWR) in Germany chose to replace 304 stainless steels with either 321 or 347 stainless steels. Nevertheless, recent study by O. Wachter and G Brümmer [2], found that six BWRs showed cracking in reactor hot water pipes where 321 stainless steels were used and one BWR which 347 stainless steels were used in reactor core component. All the observed cracks originate in the chromium carbide precipitates at the grain boundaries and in the associated chromium-depleted region near the grain boundary.
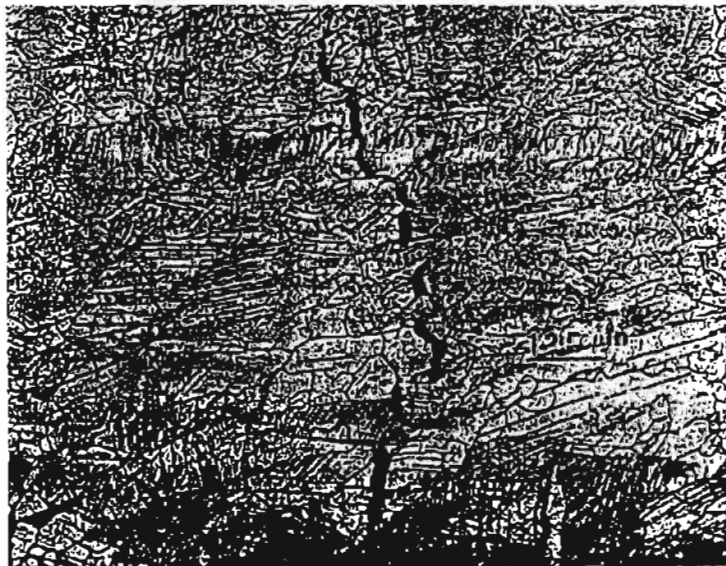
Figure 1.1 The intergranular stress corrosion cracking in stainless steels.
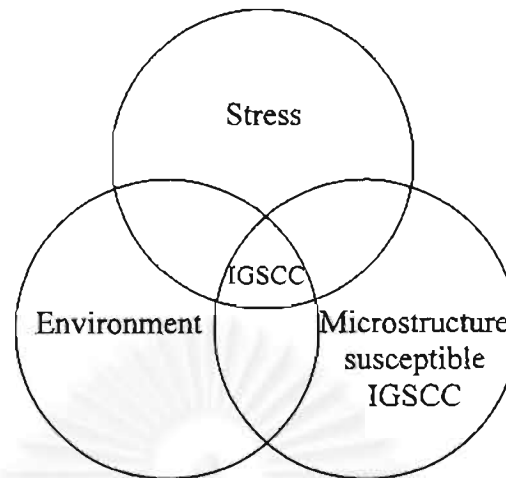
Figure 1.2 The three variables of IGSCC.

The above cases demonstrated that the use of current methods to avoid IGSCC do not entirely eliminate the existing problems of IGSCC. A study by V Thaveeprungsriporn et al. [3] indicated that there exists a relation between the occurrence of intergranular carbides and crystallographic nature of grain boundary in stainless steels. It revealed that after sensitizing stainless steel at 650 °C for 2 hrs, most of the grain boundaries were loaded with chromium carbide. However, some of the boundaries were free from these carbides and often the carbide phase abruptly ended where the boundary was intersected by a grain of different crystallographic orientation. Subsequent analysis indicates that most of the grain boundaries decorated with intergranular carbides were mostly of high angle boundaries (HABs) while grain boundaries with no intergranular carbides were identified as coincidence site lattice boundaries (CSLBs). Figure 1.3 shows grain boundaries with and without intergranular carbides.
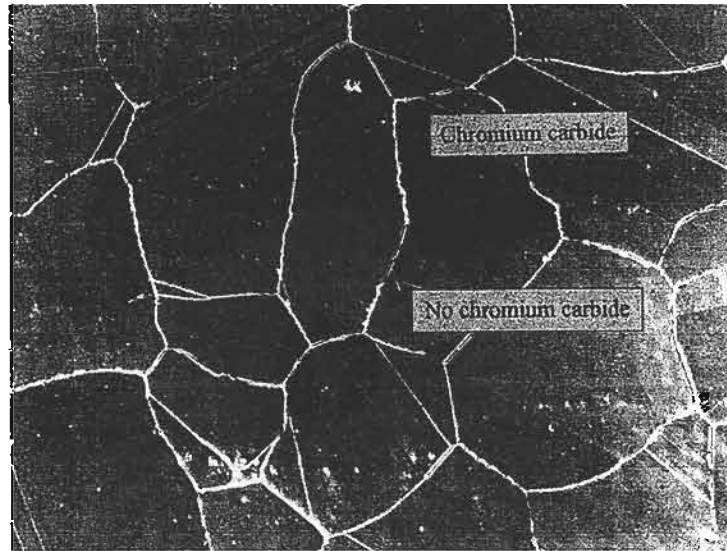
Figure 1.3 The grain boundaries with/without intergranular carbides [3].

Following the correlation between grain boundary geometry and intergranular carbide precipitation, it is therefore possible that stainless steels can be made resistant to IGSCC by increasing the CSLB population to minimize boundaries with depleted chromium and carbide precipitation. Thus, the main theme of this thesis is to attempt to increase the CSLB population in commercial 304 stainless steels.

The characterization of CSLB can be done by checking the twin boundary density which is essentially a Σ3 boundary according to the CSL model. Details of the model are described in chapter 2. It has been shown that there is a direct relationship between the frequency of CSLB and twin boundary [4]. The population of CSLB in polycrystals may thus be indirectly characterized by checking the twin boundary density. Thus, an increase in the twin density should result in an increase in the CSLB population. Figure 1.4 shows

the relationship between the population of CSLB and twin boundary. Figure 1.5 shows an example of annealing twin in polycrystalline metal.
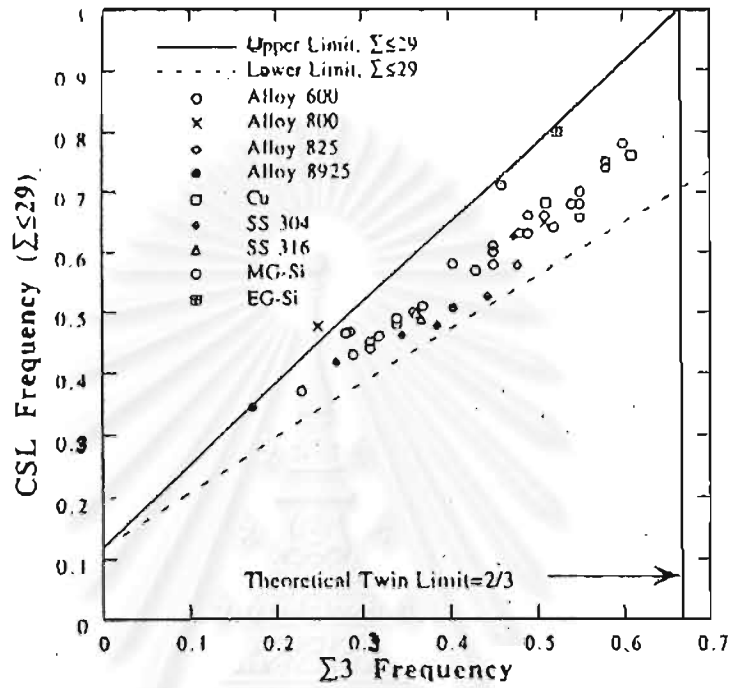
Figure 1.4 The relationship between the population of CSLB and twin boundary [4].
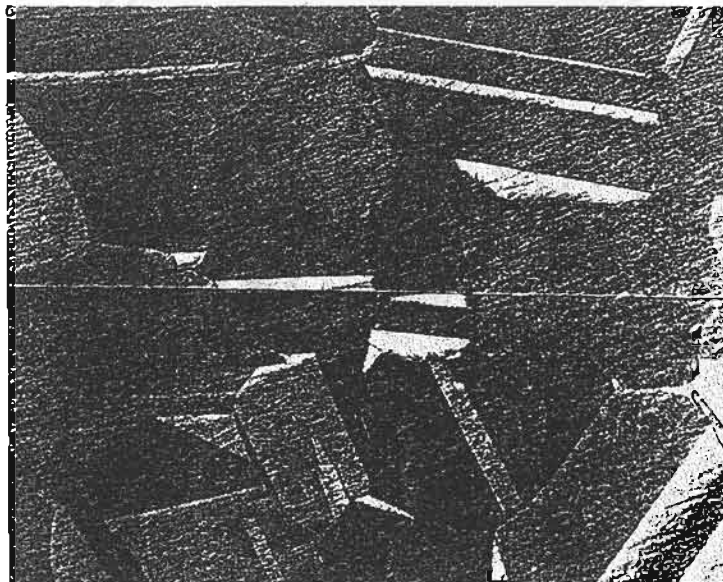
Figure 1.5 An example of annealing twin in polycrystalline metal [6].

Annealing twins can be increased by the processes which are the combination of strain and annealing and can classified in to four categories [5]: 1) iterative recrystallization, 2) one-step recrystallization, 3) iterative strain annealing and 4) one-step strain annealing.

- Iterative recrystallization, this process achieved by applied medium level of deformation then heat treatment at high temperature in a short time and repeat both processes in several times so material were retaining a small grain size and near-random texture. For example in nickel-based alloy five sequential steps of 20% cold work followed by 3 min at 1000°C resulted in grain boundary population containing 47% $\Sigma3$s and 10% $\Sigma9$s, almost double that obtained by conventional processing, Similarly, in copper strain recrystallization treatment, three steps of 30% compression and anneal at 375 °C for 10 min increased $\Sigma3$s to 58%.

- One-step recrystallization, the process of this category is short anneal at high temperature after medium levels of deformation can also produce a high twin density accompanied by small grain. For example in copper 50% deformation and 1000°C for 1 min produced higher the proportion of twin than the multi-step treatment.

- Iterative strain annealing, low level of deformation is applied, i.e. up to 6%, an increase in $\Sigma3^n$ has been found to occur during subsequent annealing without recrystallization. For example in alloy 600 (Ni-16Cr-9Fe) deformations of 2-5% followed by anneals at 890-940°C for 1-20 h have been found to increase the

proportion of $\Sigma 3$s and $\Sigma 9$s from 6 to 13% and 5 to 12%, respectively. In copper, the most successful low strain treatment was found to be 6% compression followed by 14 h at 275°C then 7 h at 375°C, the proportion of $\Sigma 3$s and $\Sigma 9$s were 67% and 9%, respectively. Although the twin fraction decreased slightly during the first anneal, it was found to be a necessary step in the evolution of the final fraction of CSLs.

- One-step strain annealing, a single anneal, either following a small applied strain or utilizing the residual strain present after recrystallization, has been observed to modify the crystallography of the grain boundary population. Evidence is available both from the crystallographic alignment of the grain boundary plans and by producing the grain boundary population in which the $\Sigma 3''$ boundary are nearer to the exact CSL configuration.

This thesis will focus on the iterative strain annealing technique to promote the CSLB population in order to minimize grain growth and recrystallization processes due to the thermomechanical treatment.

1.2 Objective

To study the effect of temperature/time to the formation of annealing twin during recrystallization and grain growth process in 304 stainless steel.

1.3 Scope of Thesis

1.3.1 To study the effect of recrystallization and grain growth process on the formation of annealing twin

1.3.2 To provide the correlation between time/temperature for the recrystallization and grain growth to twin density in 304 stainless steel.

1.4 Methodology

1.4.1 Conduct literature search and review.

1.4.2 Provide time/temperature for recrystallization and grain growth.

1.4.3 Check twin density in 304 stainless steel after recrystallization.

1.4.4 Induce the grain growth process in the recrystallized samples.

1.4.5 Check twin density of the samples after the grain growth process.

1.4.6 Determine the grain boundary character distribution.

1.5 Potential application of the thesis

Obtain time and temperature which increase annealing twin to improve the resistance of IGSCC property in 304 stainless steel.

1.6 Related research

1. In 1989, J Mizera and J.W. Wyrzykowski [6] researched on an analysis of twin boundary on mechanical properties of austenitic steel. It showed that the increasing annealing twin boundary decrease the strength of austenitic steel. However, this research had no control the another factor i.e., impurity etc., no solution annealed the austenitic steel in the experiment and had a few data on this experiment.

2. In 1987, R.A. Varin and J. Kruszynska [7] researched on control of annealing twin in type 316 austenitic stainless steel. It revealed that the number of coherent twin boundary per grain increase linearly with grain size 0.1 mm up. There are correlation between grain size and annealing temperature so the number of twin boundary per grain linearly relate to temperature and twin boundary increase during grain growth.

3. In 1997, E.M. Lehockey, G. Palumbo and A.M. Brennenstuhl [8] researched on the relationship between grain boundary character distribution on an intergranular corrosion. It showed that the intergranular damage required precipitating grain dropping is significantly greater than intergranular crack propagation. Hence, increase

the special boundary in material may be improving resistant to grain dropping and material containing special boundary greater that 50% resistant to corrosion.

CHAPTER II

THE FORMATION OF ANNEALING TWIN

2.1 Introduction

Over the last decades, metallurgists have shown increasingly interest in improving the properties of material via grain boundary engineering, and annealing twin density is one of the microstructures which has been shown to improve the corrosion resistant in stainless steel. In this chapter we will describe the models were proposed to explain the formation of annealing twin. Metallurgical parameters which may affect the twin density is also presented.

2.2 Grain Boundary Geometry

Grain boundary is the region where two crystals differ in orientation contact each other. The lattice misorientation between neigbouring grains can be described in relation of misorientation angle and axis which leading to a coincidence-site-lattice model (CSL). There are three categories grain boundaries in CSL model [3]: 1) low angle boundaries (LABs) are those boundaries with misorientation angle up to approximately 15°, 2) high

angle boundaries (HABs) are boundaries with misorientation angle greater than 15°, and 3) Coincidence-site- lattice boundaries (CSLBs) corresponds to the specific rotation of one lattice relative to the other yielding a three dimension atomic pattern in which a certain faction of lattice point coincidence: however, there are HABs fall or near CSL misorientation. In transmission electron microscope studies have shown that a few degree deviation away from an exact CSL which CSL structure can be preserve by an array of dislocations, secondary grain boundary dislocations. The maximum allowable deviation away from CSL used the Brandon's criterion is:

$$\Delta\theta = 15 \times \Sigma^{-1/2}, \tag{2.1}$$

where $\Delta\theta$ is the deviation angle from the exact CSL and Σ the reciprocal density of coinciding sites. Generally, low Σ boundary ($\Sigma < 49$) defined as special boundary which display improved physical and chemical properties such as possess lower energy, less susceptible to solute segregation, smaller diffusion, greater resistance sliding, cavitation, localized corrosion and fracture [3]. Figure 2.1 show and example of Σ boundary.
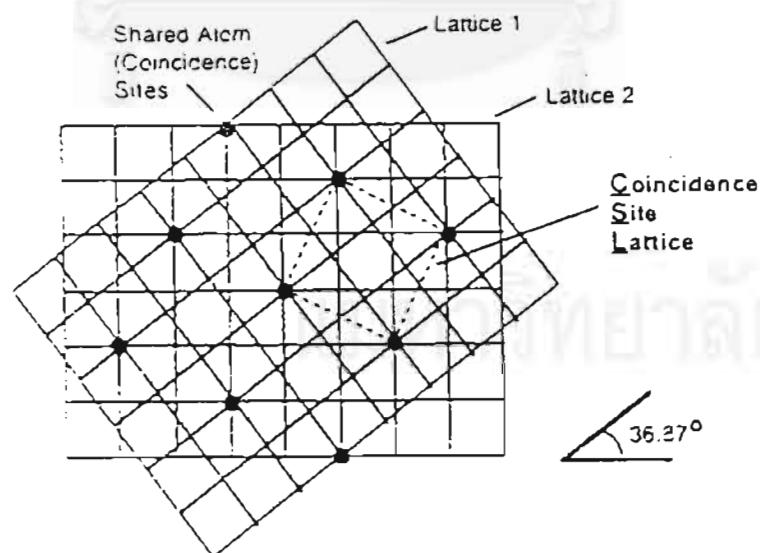
Figure 2.1 The misorientation of the $\Sigma5$ boundary [3].

2.3 Models of Annealing Twin Formation

At present, the mechanism controlling the formation of annealing twins is not yet clear despite many theories and models proposed. The models of annealing twin formation were classified into 4 group [9]: 1) the growth accident model, 2) grain encounter model, 3) stacking fault packet at migration boundary, and 4) grain boundary dissociation.

1) Growth accident model suggested that a coherent twin boundary was formd at a migrating grain boundary due to stacking error during growth under energetically favorable condition [10]. The schematic show the process of annealing twin formation in growth accident model was shown in figure 2.2.
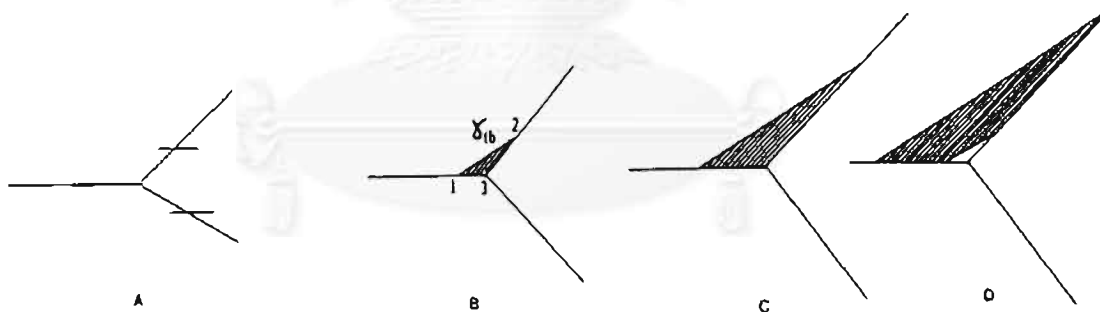
Figure 2.2 The sequence of annealing twin formation in growth accident model [9].

2) Grain encounter model suggested that the two hatched grain are at a twin orientation and in general growth process, boundaries continues migrate until touch each other then the boundaries form coherent twin boundary which minimize the systemic

energy. The schematic show the sequence of annealing twin formation in grain encounter model was shown in figure 2.3.
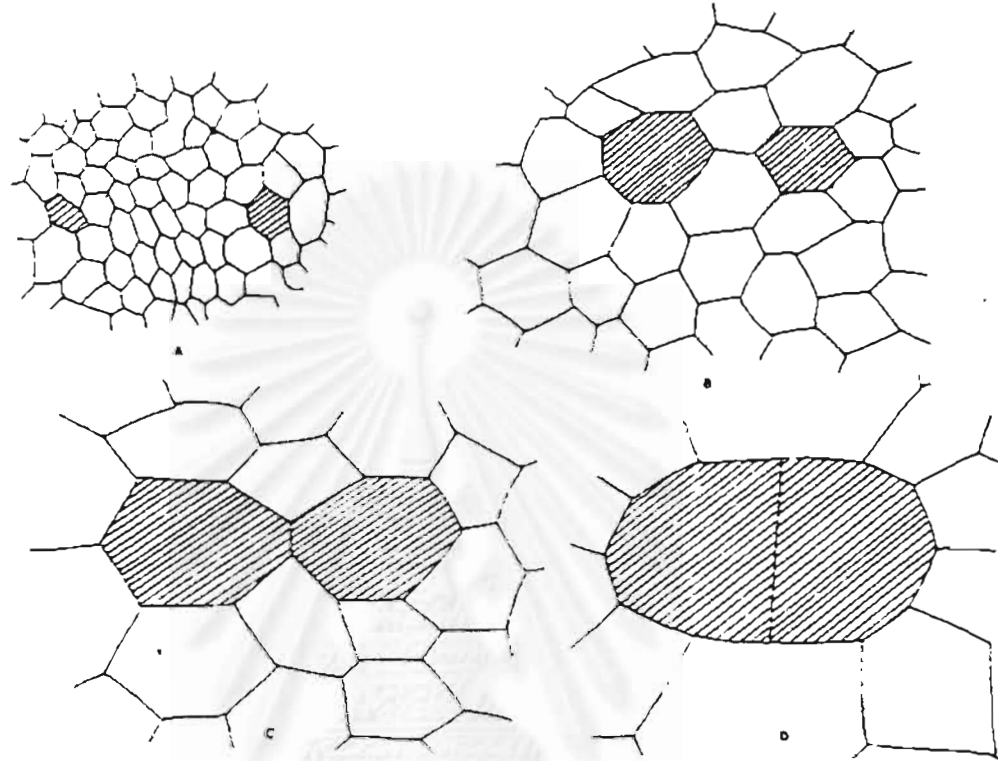
Figure 2.3 The sequence of annealing twin formation in grain encounter model [9].

3) Stacking fault packets at migration boundary proposed that the packets of stacking fault were formed during recrystallization then this stacking fault packet coalesces to produce annealing twin and this twin were grown by the movement of boundary. The schematic show the sequence of annealing twin formation in stacking fault packets at grain boundary model was shown in figure 2.4.
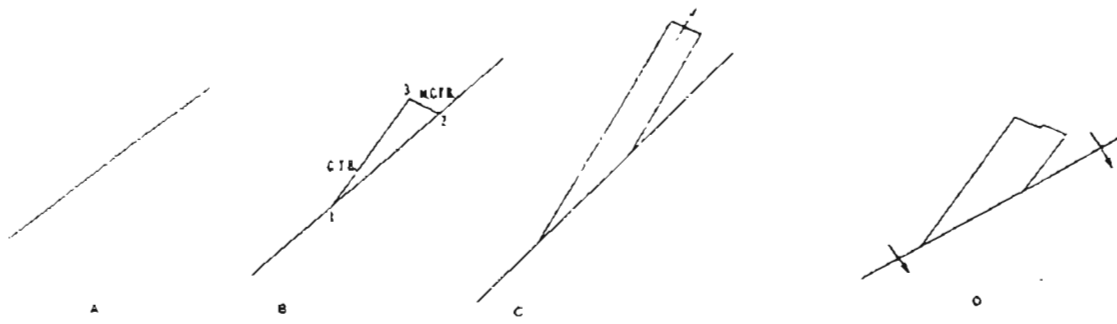
Figure 2.4 The sequence of annealing twin formation in stacking fault packets at migration boundary model [9].

4) Grain boundary dissociation, suggested that this model takes place in order to decrease overall interfacial energy, the mechanism no associated grain boundary migration was required and the boundary pop-out into 3 segments which two segments were became coherent and non-coherent twin boundary. For the energetically favored the other one segment was became a special boundary which is the low-energy boundary. The schematic show the sequence of annealing twin formation in grain boundary dissociation model was shown in figure 2.5.
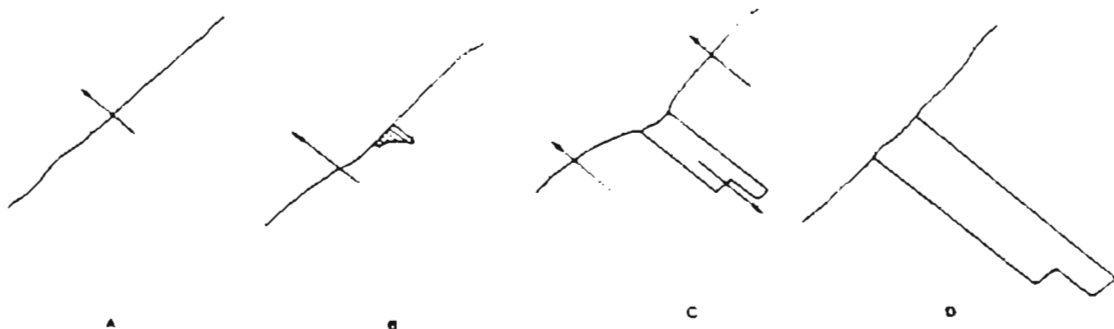
Figure 2.5 The sequence of annealing twin formation in Grain boundary dissociation model.[9]

In addition to the four models above, the mechanisms proposed can be categorized either as a grain growth model or a recrystallization model. Fullman and Fisher [11] proposed that annealing twin formed during grain growth when the free energy of the boundaries between a grain's neighbors and its twin would be less than that of the boundaries between the neighbors and the grain itself. A twin boundary might then form in a corner of a growing grain and extend as the grain continues to grow as twin of the original crystal. Their model was confirmed by using OFHC copper bus-bars 0.2 inch in thickness annealed at 500 °C for one hour and compression rolled in accordance with one of two rolling schedules as follows: (1) Compression roll to 0.020-in. thickness, with two intermediate anneals at 600 °C. (2) Compression roll to 0.025-in. thickness, with no intermediate anneals. Specimens prepared by either of these schedules were then annealed for 18 hours at 1040 °C. The result showed that the formation of annealing twins at moving grain corners, of the proportionality of twin boundary spacing to the grain size being consumed during growth. Nevertheless, their experiments did not convincingly show that twin in grain corners occurred during grain growth. On the other hand the later work by Gindraux and Form [12] proposed that the formation of annealing twin occurs mainly during recrystallization and annihilated during grain growth. They used an oxygen-free copper (99.92% Cu) having a stacking-fault energy (SFE) of ~ 70 mJ/m^2 and aluminium bronze (93.70% Cu, 6.22 Al) with an SFE of ~ 10 mJ/m^2. These materials were subjected to a homogenizing treatment of 770 °C for 15 hr in a salt bath and then deformed by 30% reduction in area in a swager. The conclusions were (1) the formation of annealing twins occurs to an overwhelming extent during recrystallization of a deformed matrix. (2) The formation of twins requires the movement of newly formed grain boundaries. (3) During recrystallization a small proportion of the newly formed

twins disappear again. (4) During grain growth the twins are progressively annihilated, either through the sweeping over of a grain boundary, or through self-destruction by movement of the non-coherent twin boundary and the extent of formation of new twins during annealing phase is very small. (5) A marked variation of stacking fault energy leads only a relatively small variation in twin density. (6) Independent of initial grain size and amount of cold work, the ratio of the number of the twins in two samples is inversely proportional to the ratio of the corresponding recrystallized grain sizes. However, their experiments were focused onto the total number of twin boundary which could be influenced by the number of grains in a specified area.

2.4 Effect of Metallurgical Parameters on the Annealing Twin Formation

Although there are some certainties in the experiments to support the two school of thoughts, it is well accepted that the formation of annealing twin can be greatly affected by several metallurgical parameters such as; temperature, cold work, purity, stacking fault energy, annealing time and initial grain size, etc.

2.4.1 Temperature

Temperature is the factor which is important in annealing twin but the result is not clearly defined since it has contrary results in each research. Pande, Iman and Roth [10], investigated the formation of annealing twin in nickel 99.9% pure, trace impurities consisted of Al 0.02%, Bi 0.02%, Cr 0.01%, Cu 0.01%, Fe 0.04%, Mg 0.01%, Mn 0.09%, Si 0.01% and Ti 0.006%, all in wt percent. Specimens were subjected series of cold

working and final heat treatments in the range of 750 °C to 1200 °C with time ranging from 2 min to 100 hr. It was found that irrespective of annealing twin temperatures and time, twin density is solely determined by the final grain size. On the other hand, the study by Form and Gindraux and Mlyncar [9] using three materials: nickel (99%), Cu-Al alloy (96.9%Cu-3%Al) and OF copper (99.95%). After homogenization at 800°C, all specimens were subjected to a cold-work/annealing cycle to reach the desired grain size before being drawn by various amounts. The result indicated that the twin density increases with increasing recrystallization temperature.

2.4.2 Time

The effect of time to annealing twin was observed by Randle [14]. It was revealed that the specimen with rapid heating to 1000° C has more twinning than specimen with slow rate heating to 1000° C. Meyer and McCowan [9], used Ni-200 alloy cold rolled to a 90% reduction and annealed was to show that twin density increases with annealing time at a certain temperature.

2.4.3 Purity

Varin and Kruszynska [7] studied the effect of impurity to annealing twin. Two commercial type 316 stainless steels with different carbon contents were used in this investigation. The latter was remelted with boron to achieve boron content of about 30-40 ppm. To ensure the same initial structure of boron free 316L the second batch was also remelted but without any boron addition and subsequently both ingots (boron and boron free) underwent the same processing with the following steps: (a) place in a furnace at 1215°C; (b) remove from the furnace after 2hr and forge to ~ 100 mm. wide and ~ 76

mm. thick at 1000 °C; and (c) return immediately to the furnace 1 hr; (d) hot roll in eight passes down to the final thickness ~ 20 mm. The results show that increase carbon content and doping with boron in austenitic stainless steels 316L suppress the formation of twin boundary.

2.4.4 Cold-work

In study the by Gindraux and Form [12], it was found that independent of amount of cold work, the ratio of the number of twins in two samples is inversely proportional to the ratio of the corresponding recrystallized grain size. However, in study by Schweizer and Form [15], it was revealed that the driving force for recrystallization is the energy stored in the cold-worked state, mostly in the form of dislocation energy. Recrystallization thus constituted that phase of annealing during which the dislocation density is reduced to an extremely small fraction of the amount present in the initial cold-worked material by the movement of newly formed grain boundary.

2.4.5 Stacking fault energy

In study by Gindraux and Form [12], is results showed that the stacking fault energy has no direct bearing on the twin frequency, whereas in the study by Gertsman and Janecek [16], the materials in their work were 316L stainless steel, two microstructural states of the steel with average grain sizes of 5 μm and 12 μm were obtained by 1-hr anneals at 1198 K and 1323 K. The result reported that f.c.c. materials with low stacking fault energy which are prone to annealing twinning.

2.4.6 Grain size

Grain size is the factor which is widely studied and the results mainly indicate that grain size affects the formation of annealing twin. In the study by Varin and Kruszynska [7], it was revealed that the number of coherent twin boundary per grain increase linearly with grain size and this dependence applied to grain sizes larger than 0.1 mm. In the range of ultrafine and fine grain size (1.5 – 100 μm.) the number of twins per grain is the lowest one and it does not virtually depend on grain sizes in the range between 50 μm and 100 μm. grain sizes.
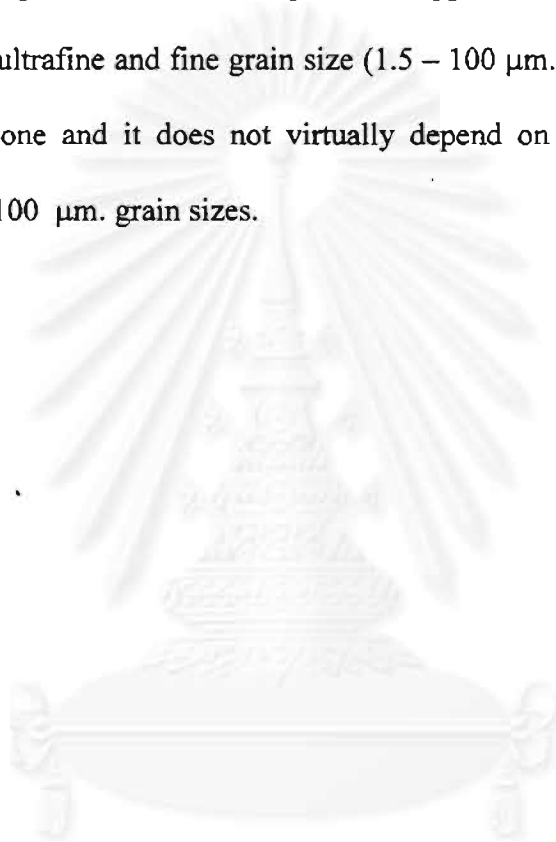
CHAPTER III

AN ELECTRON BACK-SCATTERING DIFFRACTION SYSTEM

3.1 Introduction

In this thesis, we aim to improve the intergranular properties of 304 stainless steel via grain boundary engineering by increasing the CSL boundary population. Thus, a technique to characterize grain boundary is needed to evaluate the grain boundary character distribution. In this chapter, we briefly describe the Electron Back-scatter Diffraction (EBSD) system as the technique to investigate the grain boundary structure. The EBSD has been accepted as the optimum technique for routine microstructure determination in Scanning Electron Microscope (SEM)[17]. The following basic diffraction concept and technique are obtained from Randle [19].

3.2 A Basic Concept of Diffraction Technique

The diffraction is a phenomenon that wave interacts with a grating and constructively interfere, this interfere is manifest in the measurement and acquisition of the diffraction pattern. The electron back-scatter diffraction or Kikuchi electron

diffraction pattern occurred when high energy electrons are elastically scattered by the atomic planes of crystal sample and this phenomenon was described by S. Kikuchi in 1928[18].
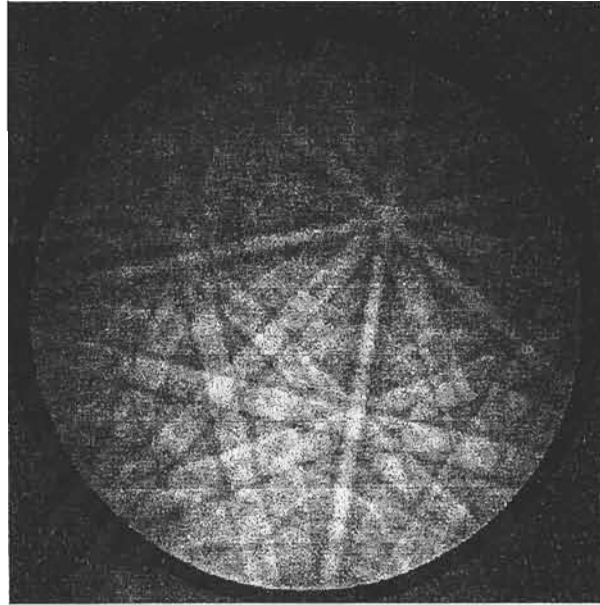
Figure 3.1 The electron back-scatter diffraction pattern.

The Kikuchi electron diffraction in SEM is a consequence of the scattering of the incident electron beam in all directions during its penetration of the thick specimen. This means that there is always a proportion of scattered electrons which impinge on all lattice planes at the Bragg's angle; these electrons are then diffracted according to Bragg's law:

$$2d \sin \theta_B = n\lambda, \qquad (3.1)$$

where d is the interplanar spacing for a family of plans, λ is the electron wavelength, n is the order of reflection and θ_B is the Bragg angle. Bragg diffraction occurs from the planes

which are on both sides of the scattering source, giving rise to two cones of electron radiation for each family of lattice planes. Figure 3.2a and b show Kikuchi diffraction in two and three dimension respectively for a single set of lattice planes. If a flat surface such as a screen or piece of photographic film is placed so as to intercept the cones of diffracted radiation, each family of planes in the crystal is represented by a pair of conic sections. The conic sections approximate to pair of straight parallel lines rather than curves because in reality Bragg angles are much smaller that shown on the schematic representation on figure 3.2, typically about 0.5°, and so the apex angle of the cones is extremely large. The line pairs which are known as Kikuchi lines, consist of a line which is darker than the background and the one which is brighter. This is due to the unequal transfer of electrons along each cone surface. The darker cone arises because fewer electrons are scatted in this direction since it makes a larger angle of scattering with the primary electron beam, and vice versa for the brighter line. This is illustrated on figure 3.2b. Only electrons which are elastically scattered through the Bragg angle contribute to the Kikuchi lines; inelastically scattered electrons form a diffuse background to the pattern [19].
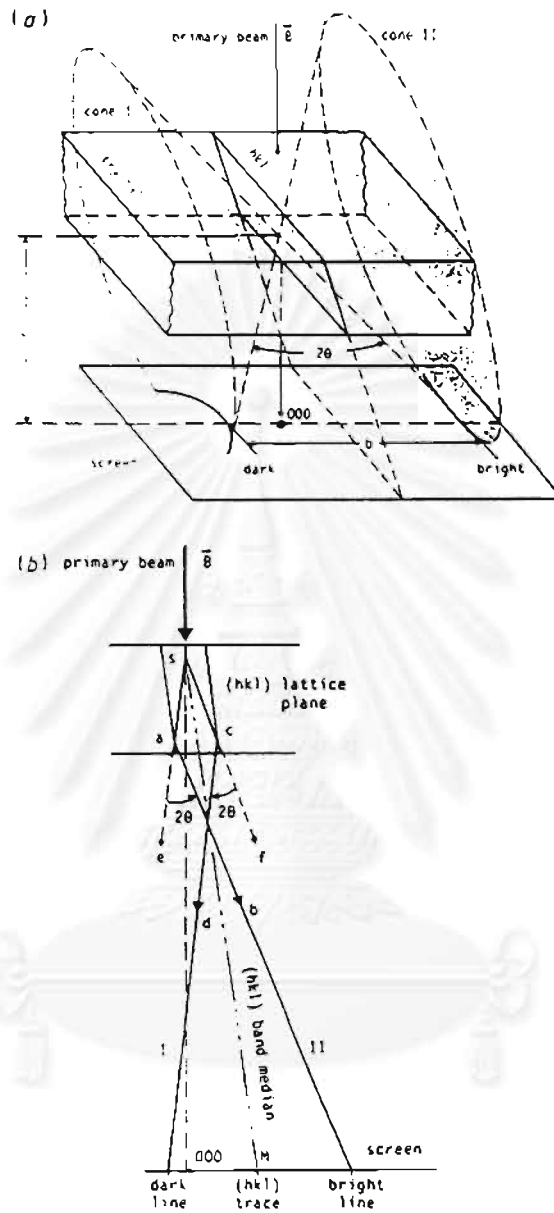
Figure 3.2 Schematic illustration of the formation of Kikuchi line pairs during diffraction (a) Three-dimensional view showing that Kikuchi lines arise from cones of diffrcted electron. (b) Two-dimensional view showing the formation of a dark and bright line [19].

3.3 An Operation Unit

The basic requirement is a highly tilted specimen, a low-light TV camera interfaced to phosphor screen. As an electron beam is focused onto the specimen mounted on a high tilted specimen, diffracted beam is projected onto a phosphor screen where the low-light camera is used to view the diffraction pattern though the back of the screen. The real-time picture of the pattern is then viewed on a monitor and analyze using a computer driven cursor and dedicated software. The unit of EBSD operation shown in figure 3.3.
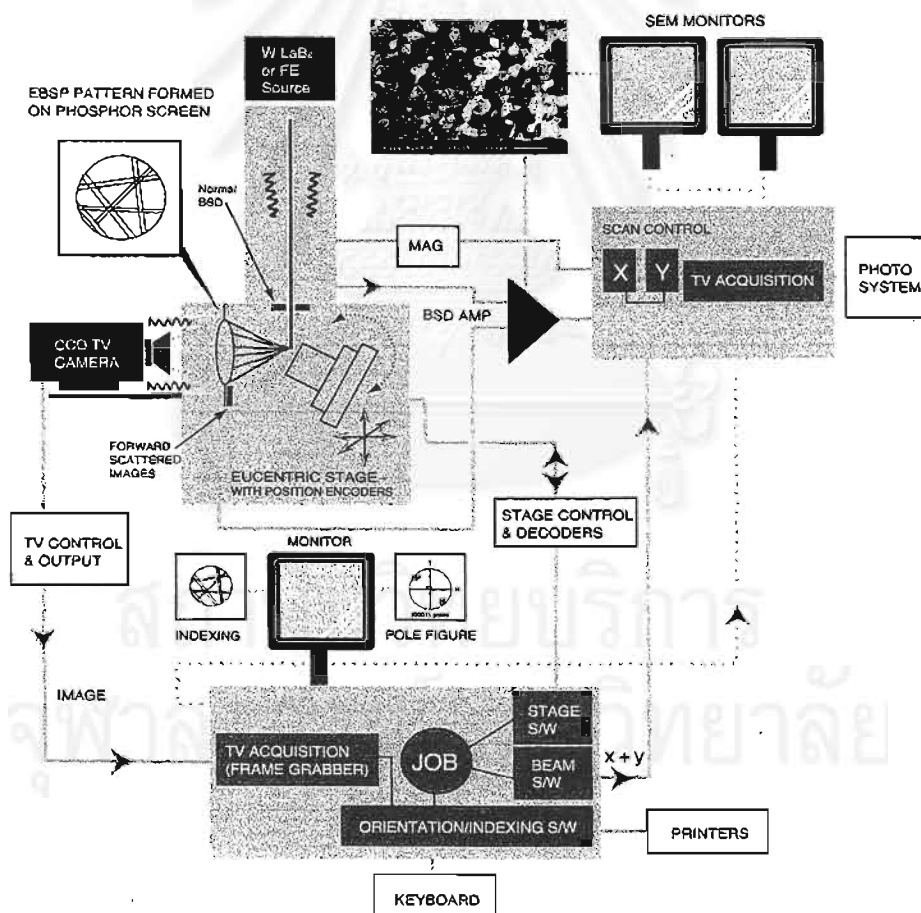
Figure 3.3 the EBSD setup

3.4 Specimen Preparation

When preparing an EBSD specimen, the objective is to remove any surface deformation and contamination the penetration depth is so small, clearly surface contaminate, such as oxide layer or impurity must be removed. It is definitely known as a general guideline for preparation of metallic materials that the surface damage introduced by conventional metallographic grinding and mechanical polishing is not suitable as a final preparation for EBSD because it introduces too much residual damage into the surface. As a final step the specimen had to be either chemically etched, electropolished or polished in a colloidal suspension of 20 nm silica particles in an alkali solution. The etchants and electrolytes used are standard types for materials.

3.5 General Operation of the EBSD Systems

The first stage in the operation of EBSD is to mount the calibration crystal and specimen into a specially designed holder pre-inclined at an angle 70.5° to the horizontal and then insert this assembly into the microscope chamber. Many holders are designed to accommodate a standard metallographically mounted specimen, figure 3.4. The precise tilt angle of the holder is a necessary part of calibration routine.
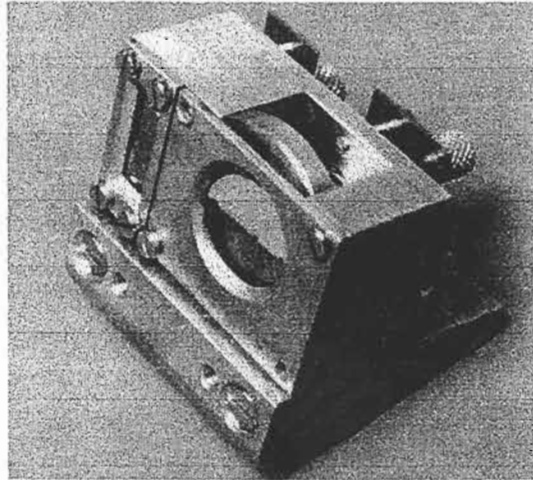
Figure 3.4 An example of sample holder with slots for both the specimen

and the calibration crystal [17].

The selected area for investigation is under operator control and will depend on what information is being sought. The most simple case is where a population of orientation is to be collected from a chosen region of the specimen without reference to stereological parameters concerning grains in the population.

The diffraction pattern and image are analyzed in a complementary way, the data become much more powerful because now orientations can be ascribed to individual grains and related to both macroscopic and microscopic features on the specimen. The image of a specimen mounted in the pre-inclined holder appears to be squashed vertically when viewed on the microscope screen due to the high tilt angle needed for EBSD. Furthermore, the extreme tilt means that only one thin horizontal strip of the image can be in focus at any time.

Once a region of interest has been located in a specimen, a diffraction pattern is obtained by siting the probe at the central point on the image, with magnification $>\times 1000$,

turning off the scan coils, then switching in the low-light TV camera whereupon the pattern is transmitted to TV monitor. As short a working distance as possible is desirable to minimize focussing distortions. Decreasing the tilt angle between the range 75-60° improves resolution somewhat, although such a decrease in tilt angle is accompanied by a decrease in the proportion of back scattered to absorbed electrons and so a tilt of 70° is a good compromise value.

The depth resolution of the diffracting volume is more than an order of magnitude smaller than the lateral resolution, that is, 10-20 nm; electrons which penetrate deeper into the specimen than this are not able to undergo back scattering. Those electrons which penetrate into the specimen form the secondary electron signal and reduce the signal to noise ratio in the diffraction pattern. Consequently, as small a penetration depth as possible is desirable, which generally means reducing the accelerating voltage for light elements.

3.6 Calibration

Accurate calibration of the system has proved to be the major technical challenge in implementing EBSD to measure orientations with the acceptable accuracy. The conventional calibration method at present utilizes a silicon single crystal, cleaved to show (001), and a purpose-built holder, accurately inclined at 70.5° to the horizontal. This geometry means that the 114 direction from the silicon crystal is horizontal, because the angle between [001] and [114] is 19.5° which is the complement of the inclination angle of holder, as illustrated on figure 3.5a. There are various refinements to this method and

also other methods which do not utilize a special crystal. One alternative method to the standard silicon calibration involves moving the phosphor screen between two positions and recording the coordinates relative to the screen at least three poles for each of two positions. The pattern center (beam normal, BN) is then defined by the intersection of three lines joining the 'before' and 'after' position of the poles as shown in figure 3.5b.

The important point with regard to using EBSD for GB studies is that accuracy is of paramount importance. With care, a misorientation can be measured to a precision of 0.5-1.0°. However, inaccuracy in the calibration routine could degrade this precision by up to 3°, which is not acceptable if the data are subsequently to be used to identify CSL GBs or other geometrically special GBs. There are several factors which can affect the accuracy. If the silicon calibration method is used, the position of the calibration crystal and the specimen must be invariant with respect to the microscope geometry, which includes having the surface of both parallel to the inclined holder, i.e. 70.5° to the horizontal. Another consideration is the specimen height. Both the calibration and the orientation measurement routines need the specimen height as an input parameter because this will influence both the position of pattern source point and pattern center and the distance from the pattern source point to the pattern center for most microscope the specimen height is only known to the nearest millimeter, as displayed on the microscope column, which could feed though as an error of up to 1.5%.
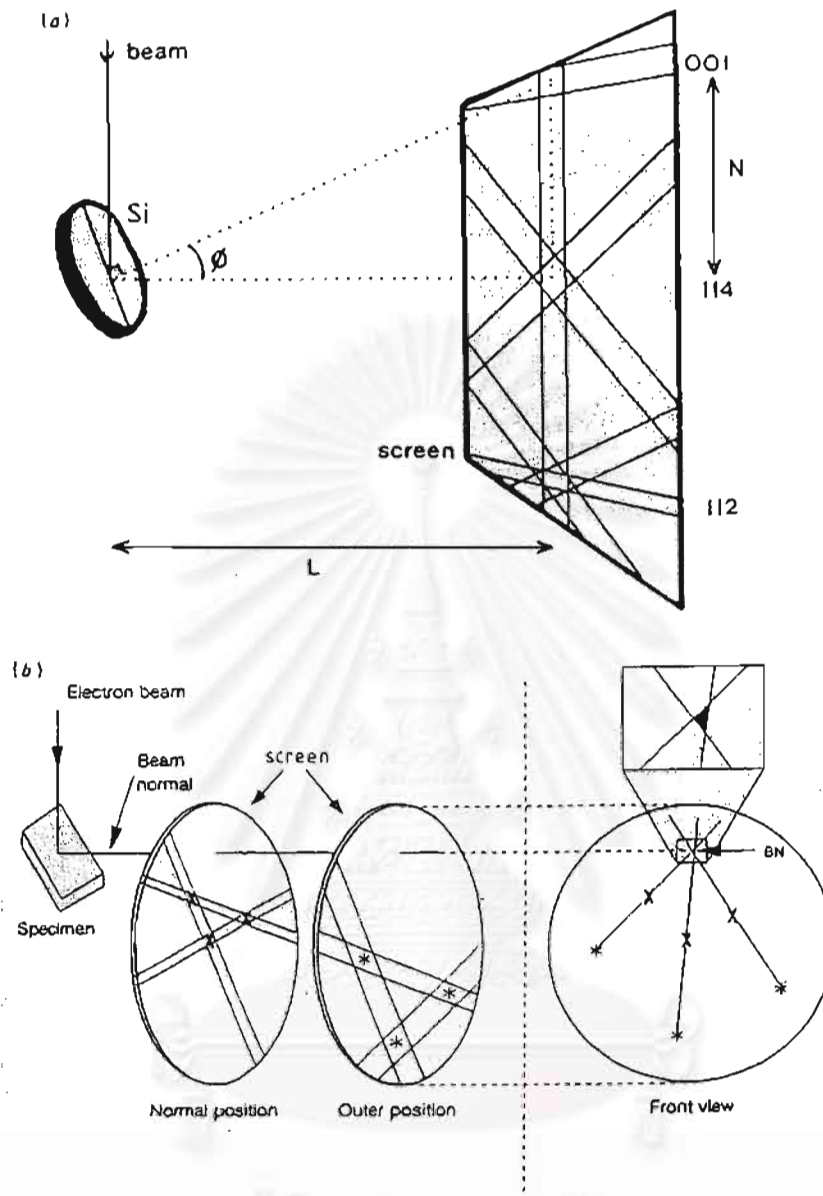
Figure 3.5 The calibration of the EBSD system. (a) Established calibration method using an 001 silicon crystal tilted at 19.5° to the beam. (b) Alternative calibration method involving moving the phosphor screen and recording the positions of the same three zone axes for both screen position [19].

3.7 Data Interpretation

in this thesis we interest in CSL fraction so in this section, the CSL misorientaion will classify. One method compares analytically the misorientation matrices for the experimental and CSL cases, M_{EXP} and M_{CSL} respectively. The difference matrix M_D is given by :

$$M_D = M_{EXP} M_{CSL}^{-1} \qquad (3.2)$$

M_{EXP} and M_{CSL} refer to the same symmetry related solution, usually the one containing the lowest angle. The angular deviation from exact CSL matching can also be obtained by calculating the average of the three angles between the 100, 010, and 100 directions in both M_{EXP} and M_{CSL}, i.e. the angles between the first, second and third column in these two matrices. Here v is given by:

$$v = (\,|\,\theta_{EXP} - \theta_{CSL}\,|^2 + (2\theta_0 \sin (\theta_{EXP}/2))^2)^{1/2} \qquad (3.3)$$

where θ_0 is the angular diffraction between $(UVW)_{EXP}$ and $(UVW)_{CSL}$.

The specification of a maximum allowable deviation that an experimental GB can have and still be classed as a CSL, v_m. Almost always the 'Brandon criterion' is adopted to give v_m. Using the Brandon criterion in the present example, v is 4.5° and $\Sigma=3$ GB gives the relative deviation:

$$v/v_m = 4.5° / 8.66° = 0.52$$

CHAPTER IV

EXPERIMENTS

4.1 Introduction

Experiments in this thesis can be separated into 2 sections. The first section deals with specimen preparations for recrystallization and strain annealing study. The other section discusses the characterization of the prepared specimen using electron back-scattering diffraction system to determine its crystallographic orientation distribution.

4.2 Specimen Preparation

4.2.1. Recrystallization study.

As received 304 stainless steel rods with a diameter of ~ 4.7 mm were cut into pieces of 2 inches long. Each specimen was then solution annealed at 1050°c for 2 hr and compressed to ~30% reduction in thickness. The solution annealed specimens were then separated into 3 groups: the first group was recrystallized at 800°c for various time ranging from 10 min, 30 min, 1 hr, 2 hr, to 4 hr. Similarly, second and third group were

instead annealed at 850 °C and 950 °C, respectively. After recrystallized and followed by water quenched, the specimens were mechanically polished down to 1 μm diamond paste and electropolished in solution containing 60%H_3PO_4 + 40% H_2SO_4, at 20 volts for 3 min. Then, the specimens were electroetched in a 10% oxalic acid solution at 6 volts for 10 second. Electron micrographs of the specimen were taken using a JEOL 5800LV SEM at STREC, figure 4.1. Informations such as grain size and twin density are of our interest. Table 4.1 shows the matrix test of recrystallization study.
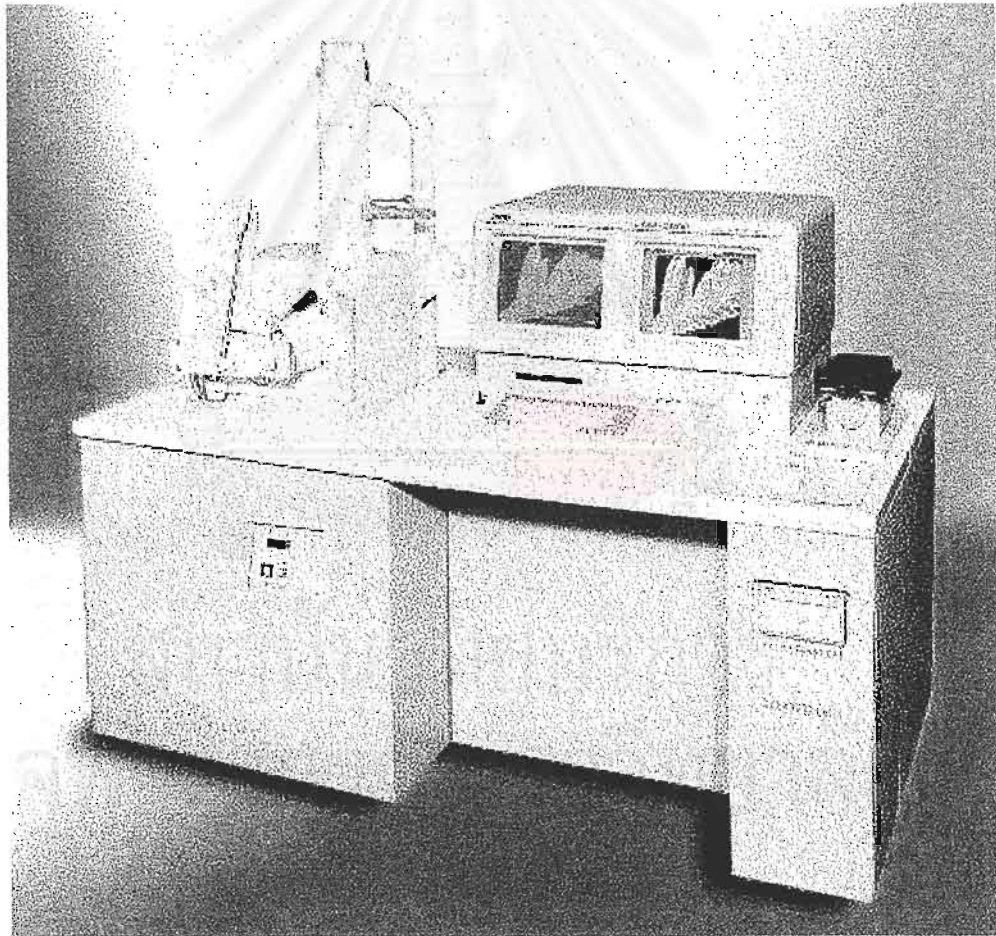
Figure 4.1 The scanning electron microscope model 5800LV.

Table 4.1 Summary of the matrix for recrystallization study.

Recrystallization temperature	Recrystallization time after 30% deformation
800°C	10 min, 30 min 1h, 2h, 4h
850°C	
950 °C	

4.2.2. Strain Annealing study

In this study three recrystallized specimens were used. the 800°C/30 min, 850°C/1hr and 950°C/4hr recrystallized specimen were cut into 3 sections, compressed by 3% reduction in thickness and annealed at 900°C, 950°C, and 1000°C for 10 min. After annealing the specimens surface was prepared for microstructure characterization by mechanical polishing down to 1 µm diamond paste and electropolishing in a solution containing 60%H_3PO_4 + 40% H_2SO_4, at 20 volts for 3 min. Then, the specimens were electroetched in a solution containing 10% oxalic acid at 6 volts for 10 second. To study the effect of iterative strain annealing, the strain annealed specimen at 950°C were used. The strain annealing of 3% deformation in thickness and heat treated at 950°C process were repeated twice. Table 4.2 shows the matrix test of strain annealing process

Table 4.2 Summary of the matrix test for the strain annealing study.

process	Sample	Recrystallized temperature (°C)								
		800			850			950		
		1	2	3	1	2	3	1	2	3
1	3%deformation	X	X	X	X	X	X	X	X	X
	900°c	X	-	-	X	-	-	X	-	-
	950°c	-	X	-	-	X	-	-	X	--
	1000°c	-	-	X	-	-	X	-	-	X
2	3%deformation	-	X	-	-	X	-	-	X	-
	950°c	-	X	-	-	X	-	-	X	-
3	3%deformaton	-	X	-	-	X	-	-	X	-
	950°c	-	X	-	-	X	-	-	X	-

4.3 Specimen Characterization

The crystallographic orientation of specimen was characterized using an automatic EBSD system under the trade name of OPAL in 5800LV SEM at the Scientific and Technological Research Equipment Center (STREC). The information from EBSD allows us to get an insight into orientation distribution and grain boundary character distribution of each specimen condition. The following procedures were used to operate the SEM, acquire and analyze the diffraction pattern using OPAL system.

1. To set up the EBSD system, we begin by launching the OPAL software in ISIS software by Oxford Instrument, then

   1.1 Selected the **analysis setup** in **edit** topic and input the operating voltage for OPAL operation at 25 keV.

   1.2 Input the material data for stainless steels, the gamma iron was used to set the material type.

   1.3 Select the new file and set the file name for our analysis.

2. Acquire diffraction was set up in the next step, this is accomplished by

   2.1 Set up the SEM condition, the operating voltage in SEM is 25 keV, the selected area was adjusted until the image is cleared, then select the **BCX** mode on SEM.

   2.2 Increase the image magnification over ×4000, click at **acquire pattern** on the computer screen in OPAL system and click on **set** button on SEM screen. The pattern was shown on the computer screen.

   2.3 Click on the **cross** button on SEM screen and reduce the image magnification, click the **acquire background** in OPAL system on computer screen and click again for leave it, then click on the **subtract background** box.

   2.4 Increase the SEM magnification, click on set button on SEM and acquire pattern again.

3. Calibration is the next step to run OPAL system, started by

   3.1 Selected the pattern which can identify zone axes, figure 4.2 shows zone axes of fcc material.

Figure 4.2 The zone axes of fcc material.

3.2 Click on the **tool** topic in OPAL system, select the **calibration** mode then the message box of *collect pattern* appeared. Click **OK** to accept it.

3.3 The message box to *move camera out of the position* appeared, move the camera out of position then click **OK**.

3.4 The message box to *move camera in position* appeared, move the camera in to the old position then click **OK**. The patterns of the camera in position and out position were shown on the screen.

3.5 The message box of the next step appeared. Select the three bands of the pattern in pattern, use control button and mouse to drag the line on the selected band, after finish this process click on **OK**.

3.6 The blue triangle and the red circle appear, if the triangle smaller and site inside the circle, this pattern can be accepted. If it is not try to move the line in each band until the triangle is smaller and site is inside the circle.

3.7 Select two zone axes which can be identify to find the angle between them by dragging the line across each zone axes. Using the arc cosine of dot product of two identified axes. If the angle is correct the straight line which has its end on the center of the across line will appear, then click **OK**.

3.8 **Acquire** the pattern after leaving from the **calibration** mode, click on the **analysis pattern** button the zone axes will appear like figure 4.2. If the zone axes are correct add the zone axes in the result. If the axes are wrong repeat the calibration step again.

4. The final part is mapping, selecting mapping subject on the OPAL system then the new window will appear.

4.1 In put the SEM data about accelerating voltage 25 keV, magnification at ×2000 - ×3000, working distance and specimen current in detail box, this detail can be seen on the display screen of SEM,

4.2 **Acquire** image and select mapping area about 0.02 mm², then software will run the characterization process by automatically characterizing the pattern.

4.3 After the characterization is completed, the characterized map will be shown. **Filter** the characterized map to reduce some unidentified patterns.

4.4 Find the misorientations were characterized by used the **misorientation** button. The misorientation histogram will be shown after the process is finished.

4.5 Find the **CSL misorientation** to finish all characterization process. Select the sigma value from 3-29, the CSL histogram will be shown after the process is finished. Figure 4.3 a and b show the secondary electron image and the image from the OPAL system.

4.6 View the result by click on the analysis result button. The results will show the
average grain size, ASTM grain size, average ECD and the amount of sigma value
of each sigma value.
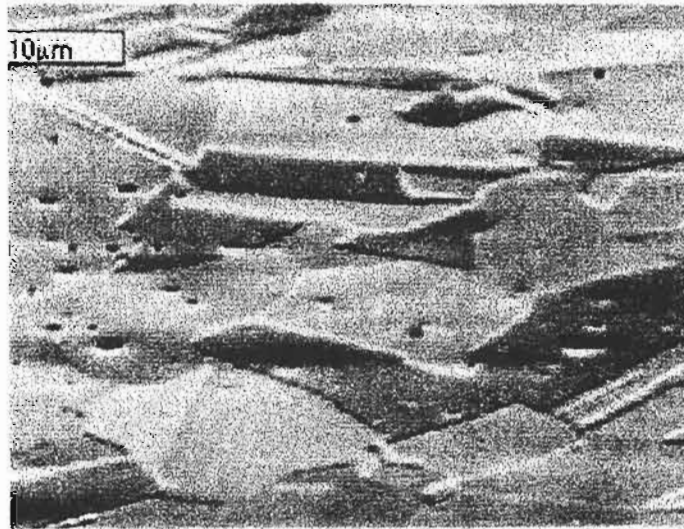
(a)
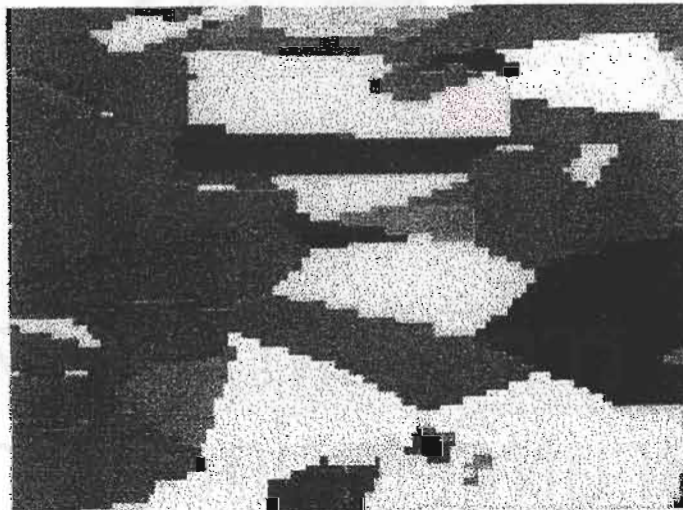
(b)

Figure 4.3 (a) The secondary electron image
(b) The image from OPAL system

CHAPTER V

EXPERIMENTAL RESULTS AND DISCUSSION

5.1 Introduction

This chapter provides the results of the experiments including the discussion and conclusion. The discussion begins with the recrystallization process followed by strain annealing and iterative strain annealing process, respectively. The objective of the discussion is related to how different processing conditions affect the twin density, and thus the CSL distribution.

5.2 Experimental Results and Discussion

5.2.1 Recrystallization process

In this recrystallization process, specimens were recrystallized at various time ranging from 800°C, 850°c and 950°c for a period of 10 min, 30 min, 1hr, 2 hr and 4 hr. Figure 5.1 shows an example of recrystallized microstructure of 304 stainless steel. The metallographic results are summarized in table 5.1, 5.2 and 5.3.
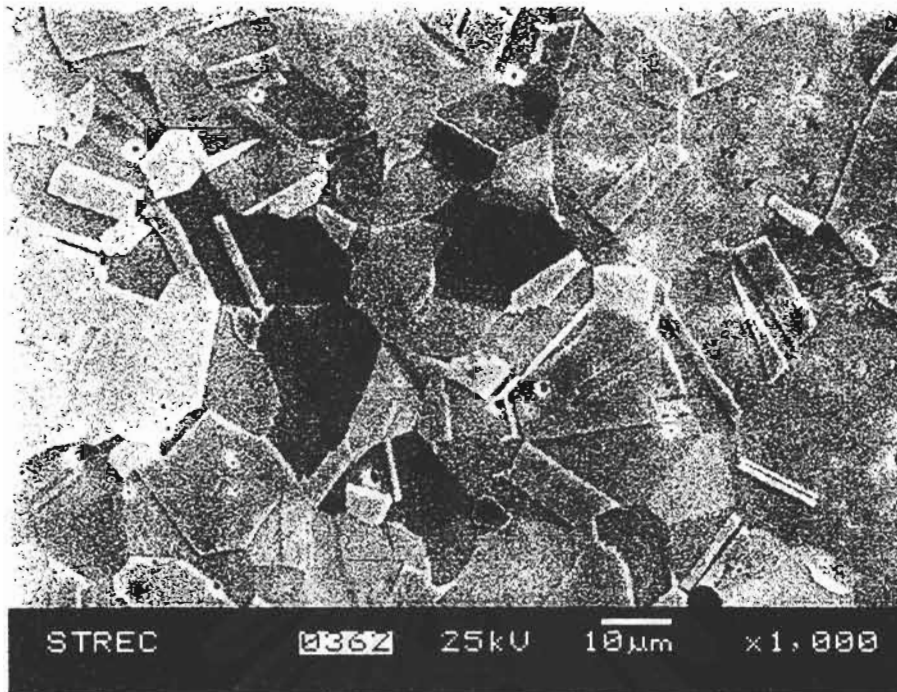
Figure 5.1 The microstructure of recrystallized 304 stainless steel.

Table 5.1 Grain size and twin density of specimens heat treated at 800°C

Time (min)	Grain size (μm)	# twin	# grain	Investigated Area (mm^2)	Twin per grain
10	10.8 ± 0.92	637	372	0.030	1.712 ± 0.27
30	13.8 ± 2.04	595	327	0.033	1.820 ± 0.14
60	14.8 ± 3.00	752	383	0.047	1.963 ± 0.25
120	16.0 ± 0.84	732	432	0.072	1.694 ± 0.22
240	19.1 ± 2.37	448	298	0.069	1.503 ± 0.21

Table5.2 Grain size and twin density of specimens heat treated at 850°c

Time (min)	Grain size (μm)	# twin	# grain	Investigated Area (mm^2)	Twin per grain
10	11.3 ± 0.58	586	365	0.030	1.605 ± 0.16
30	15.3 ± 0.77	599	420	0.072	1.426 ± 0.14
60	16.4 ± 0.96	499	356	0.068	1.402 ± 0.26
120	24.0 ± 2.50	650	426	0.120	1.526 ± 0.24
240	26.1 ± 1.89	610	344	0.120	1.773 ± 0.10

Table 5.3 Grain size and twin density of specimens heat treated at 950°c

Time (min)	Grain size (μm)	# twin	# grain	Investigated Area (mm^2)	Twin per grain
10	21.3 ± 038	532	336	0.120	1.583 ± 0.20
30	24.1 ± 1.69	521	321	0.120	1.623 ± 0.29
60	26.8 ± 1.83	485	279	0.120	1.738 ± 0.29
120	26.2 ± 2.11	428	283	0.120	1.512 ± 0.23
240	30.8 ± 3.03	540	353	0.255	1.530 ± 0.13

The results show that the grain size increases with increasing annealing time and temperature, figure 5.2.
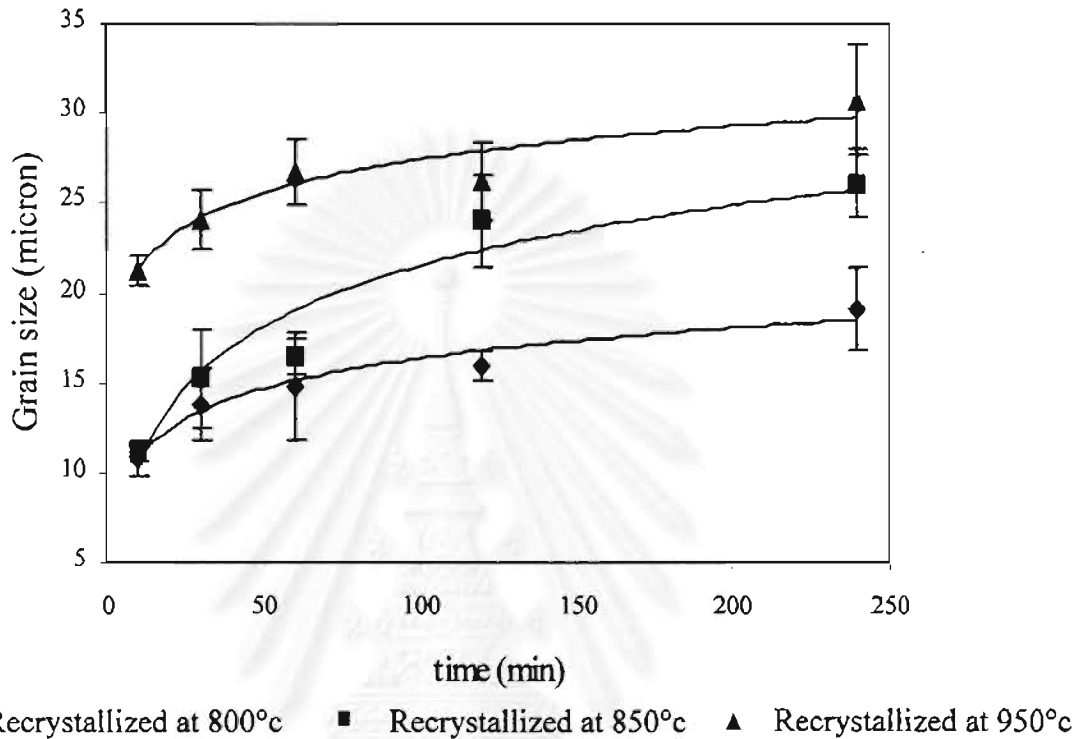
Figure 5.2 Plot showing the correlation between grain size and annealing time.

According to the grain growth kinetic, grain size can be described as a function of time by following relation [10]:

$$D = kt^n, \tag{5.1}$$

where D is the grain size, k is a constant, t is an annealing time and n is the metallurgical constant. Figure 5.3 shows the plot of ln D versus ln t and the slope is thus the n value.
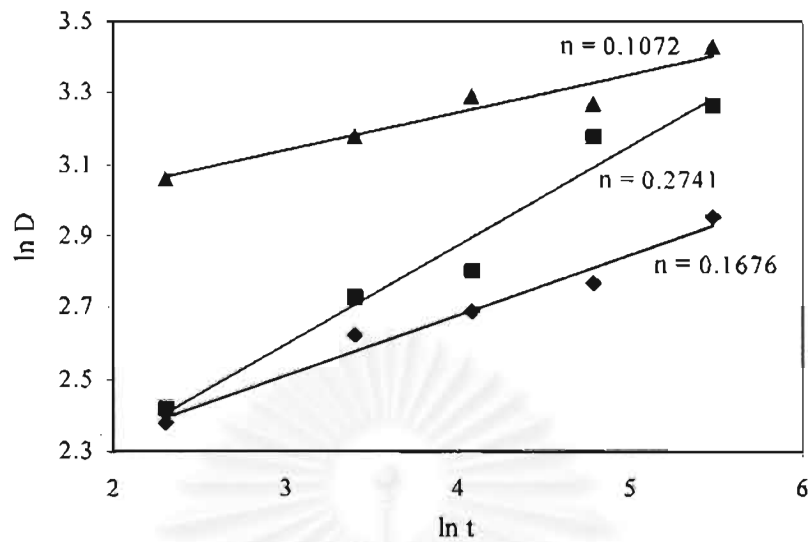
Figure 5.3 The correlation between ln grain size (D) and ln time (t).

It indicates that the specimen recrystallized at 850°C has the highest n value followed by specimen recrystallized at 800°C and the lowest n value belong to the specimen recrystallized at 950°C. According to the n value, we can expect that the grain growth rate of our specimens recrystallized at 850°C is the highest while specimen recrystallized at 800°C and specimen recrystallized at 950°C have lowest growth rate, respectively. The n values above do not signify an absolute grain growth rate per se, they represent the rate of grain growth relative to initial grain sizes. The specimen heat treated at 950°C were in a slower grain growth region due to lower driving force from a larger initial grain size.

In this thesis, we are interested in how the grain size and grain growth rate affect the twin density. It was found that the recrystallized grain size do not affect the twin density,figure 5.4.
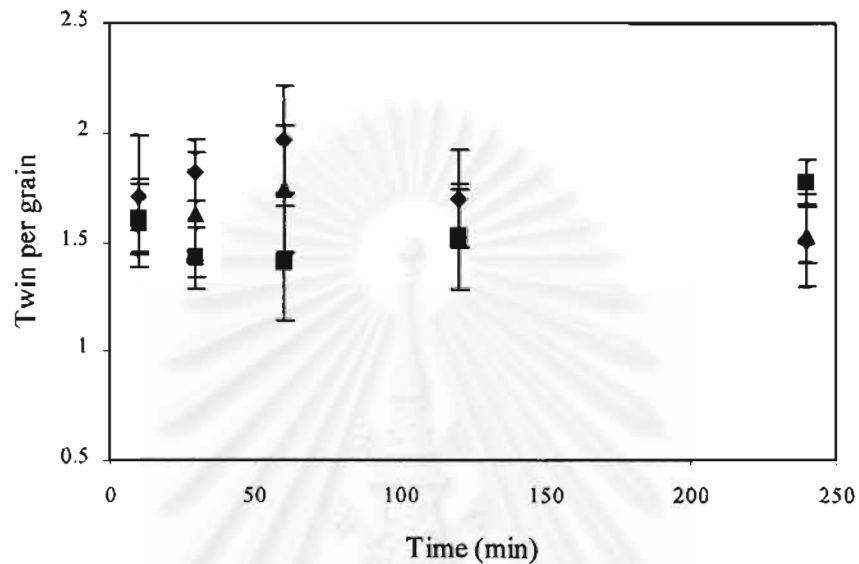
Figure 5.4 Plot showing the correlation between twin per grain and annealing time.

Following the investigation by Varin and Kruszynska on 316 stainless steel (Fe-19Cr-9Ni-Mo) [7], it was shown that twin density linearly increase with increasing grain size for grain sizes larger than 100 μm. However, their results also show that for grains formed during recrystallization which have not undergone any substantial grain growth (grain size <100 μm), the number of twins formed is the lowest one (between 0.5 and 1.0) and is relatively independent of any specific thermomechanical treatment and/or compositional changes. Their results are in agreement with this work indicating that within the investigated range of grain size less than 50 μm, twin density is independent of

recrystallized grain size. Figure 5.5 shows the dependence between twin density and grain

size for ultra fine and fine-grained material.
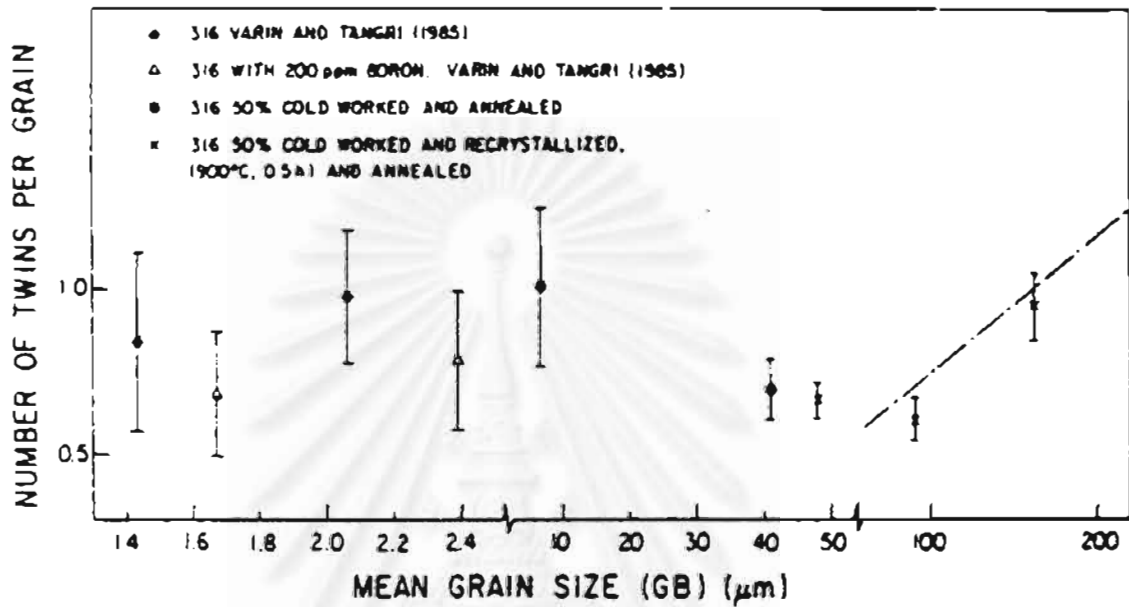
Figure 5.5 The correlation between twin density and grain size [7].

To investigate the correlation between twin density and CSL fraction, we selected

some recrystallized specimens to check for there CSL fraction. The results show that the

CSL fractions are not significantly different among twin density values investigated.

Table 5.4 shows the result of twin density and CSL distribution.

Table 5.4 The result of twin density and CSL distribution in recrystallized specimens.

Recrystallized time temperature (°C)	Twin density	Percent CSL
800/30 min	1.820	35.62
850/2hr	1.526	31.85
950/4hr	1.530	37.49

Previous research conducted by Palumbo et al. [20] on alloy 600 (Ni-15Cr- 10Fe) indicated that to reduce both the magnitude and variance in maximum intergranular cracking lengths, the special grain boundary frequencies in excess of approximately 70% are need. Figure 5.5 shows the maximum intergranular crack depth as a function of special grain boundary frequency. According to figure 5.6, a CSL fraction of ~30-40% results in a maximum crack length 6-10 times higher than what is considered immune. Thus it may be concluded that for 30-40% CSL in 304 stainless steel may not be sufficient to improve intergranular property in this material.
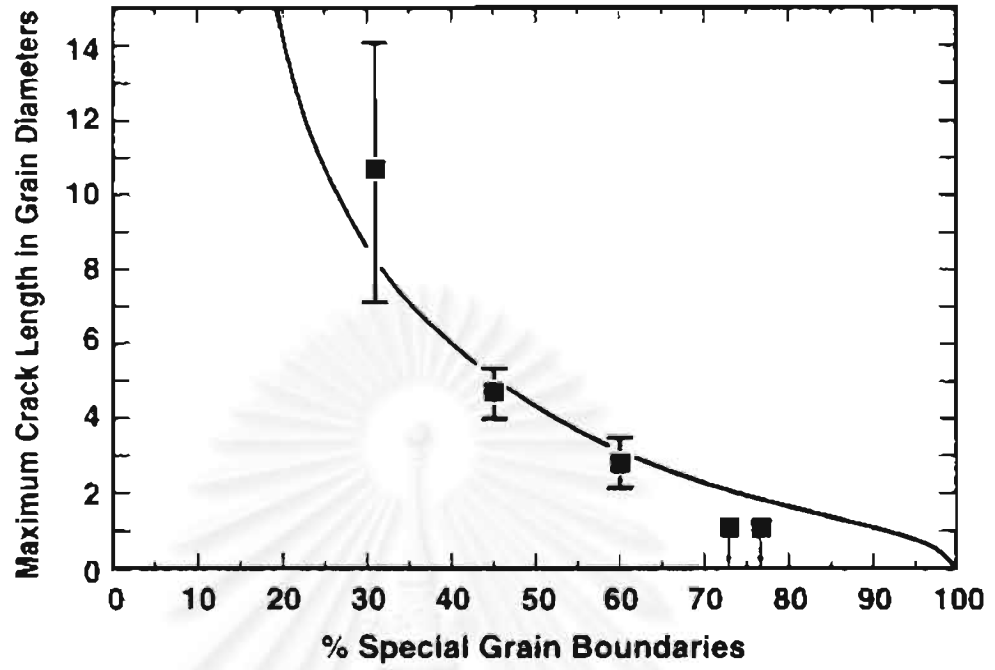
Figure 5.6 The maximum intergranular crack depth as a function of special grain

boundary frequency [20]. (Alloy 600 tested in 10% NaOH at 350°C)

5.2.2 Strain annealed process

In this section, the specimens were compressed by 3% reduction in thickness introduced as a driving force for grain boundary migration, then annealed at 900°c, 950°c and 1000°c. Figure 5.7 shows an example of strain annealed microstructure of 304 stainless steel. Table 5.5, table 5.6 and figure 5.8 shows the results of this part. Figure 5.9 shows the twin density increased with increasing grain size.
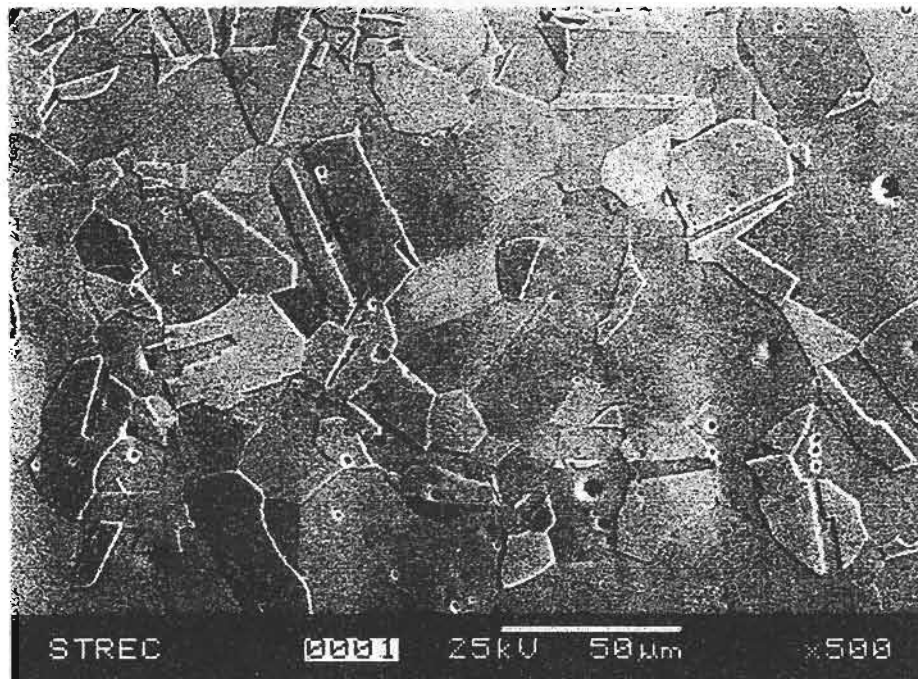
Figure 5.7 The microstructure of strain annealed specimen.

Table 5.5 Summary of metallographic results of strain annealed specimen.

Sample	Strain Annealed	Grain Size Total (μm)	Twin per Area	Total Bdry per Area	Grain per Area	Twin per Grain	Total Bdry per Grain
800°c	Initial	13.78	18030	62200	9909	1.820	5.424
	900	15.52	9403	33000	5528	1.701	5.881
	950	24.64	5967	18667	2692	2.217	6.188
	1000	34.24	2592	5783	1350	1.920	4.627
850°c	Initial	23.98	5417	17583	3550	1.526	5.172
	900	25.06	6551	18222	3319	1.975	5.513
	950	31.08	3958	9483	1850	2.140	5.126
	1000	36.02	2580	8188	1239	2.082	6.289
950°c	Initial	30.75	2118	8753	1384	1.530	6.643
	900	29.13	2517	8433	1892	1.330	4.478
	950	28.15	3608	11733	1950	1.850	6.609
	1000	37.92	2259	6408	1149	1.966	5.375

Table 5.6 Summary of the grain boundary character distribution results of strain annealed specimen characterized using the EBSP technique.

Sample	Strain annealed	Percent CSL ($\Sigma3$-$\Sigma29$)	Percent LAB	Percent $\Sigma3$
800 °C	Initial	35.62	6.26	32.17
	900 °C	34.86	4.04	28.53
	950°C	25.83	6.01	24.02
	1000 °C	46.26	4.32	42.43
850 °C	Initial	33.65	4.78	31.85
	900 °C	25.07	4.15	19.80
	950°C	44.21	2.88	42.22
	1000 °C	29.72	4.53	25.82
950 °C	Initial	38.35	5.43	37.49
	900 °C	36.46	3.77	31.82
	950°C	35.11	2.88	30.43
	1000 °C	39.10	2.86	35.53
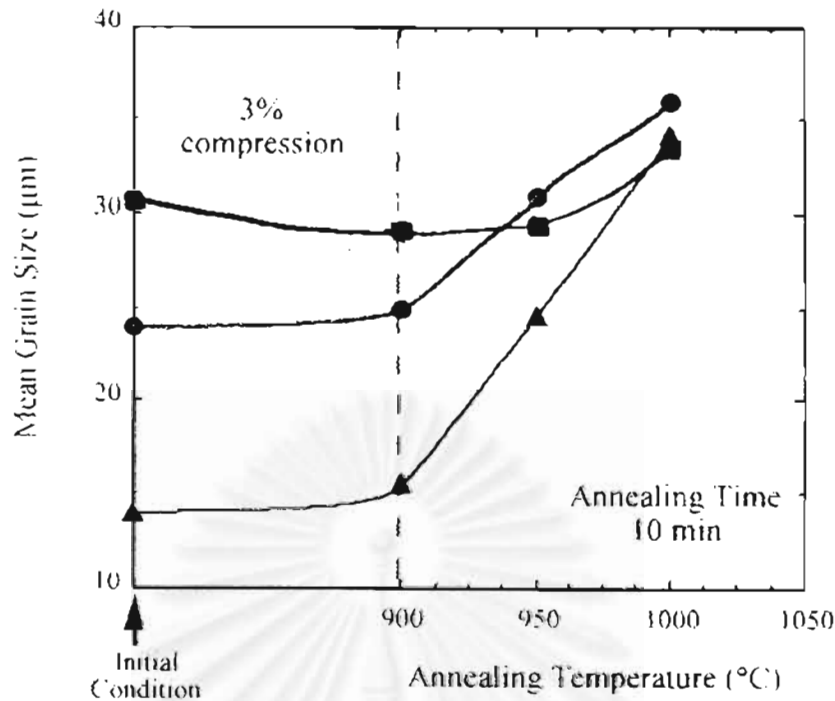
▲ Recrystsllized at 800°C ● Recrystsllized at 850°C ■ Recrystsllized at 950°C

Figure 5.8 plot of the correlation between grain size and annealing temperature.

In this study, the chosen recrystallized specimens were of different in initial grain size, but with similar in twin density. Figure 5.8 shows the effect of strain annealing on grain growth. It was found that the largest increase in grain size occurred at the annealing temperature of 1000°C. It can be seen that annealing at 900°C does not affect the mean grain size. Heat treating at 950°C and 1000°C moderately and significantly increase the grain size depending on initial grain sizes. The result is in accordance with Kurzydlowski [21] as characterized by the change in the mean grain size and subsequently either annealed for various times at constant temperature or annealed at different temperature fo fix time, figure 5.9
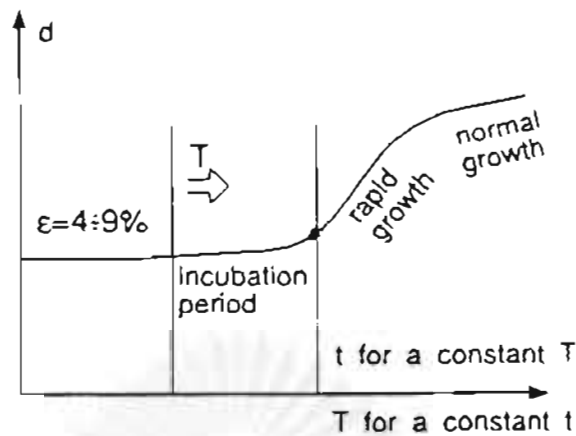
Figure 5.9 Schematic representation of the changes in the mean grain size of grains

induced by pre-straining and subsequent annealing.

Kurzydlowski pointed out that the situation of two driving force field that do not show a high degree of correlation suppress the rate of grain disappearance to the degree that for awhile it makes the changes in the mean grain size of grain negligibly slow, the effect manifested by the appearance of the incubation period. Although the combine effect of tension and strain driven grain boundary migration slow down changes in the mean grain size of grain, it does not stop local grain boundary migration as it is manifested by the changes in the value of the grain shape parameter and in grain size coefficient of variation, and the incubation period is characterized by significant activity of grain boundaries.

The correlation between mean grain size and twin per grain is show in figure 5.10. The result is not clear explainable. But by plotting the change in grain size and twin density, figure 5.11, it can be seen that twin increases with increasing grain size up until about 30% increase in grain size when the twin density starts to decrease. This may be explained by involving the concept of reduction is system energy as proposed by Gindruax and Form [12].
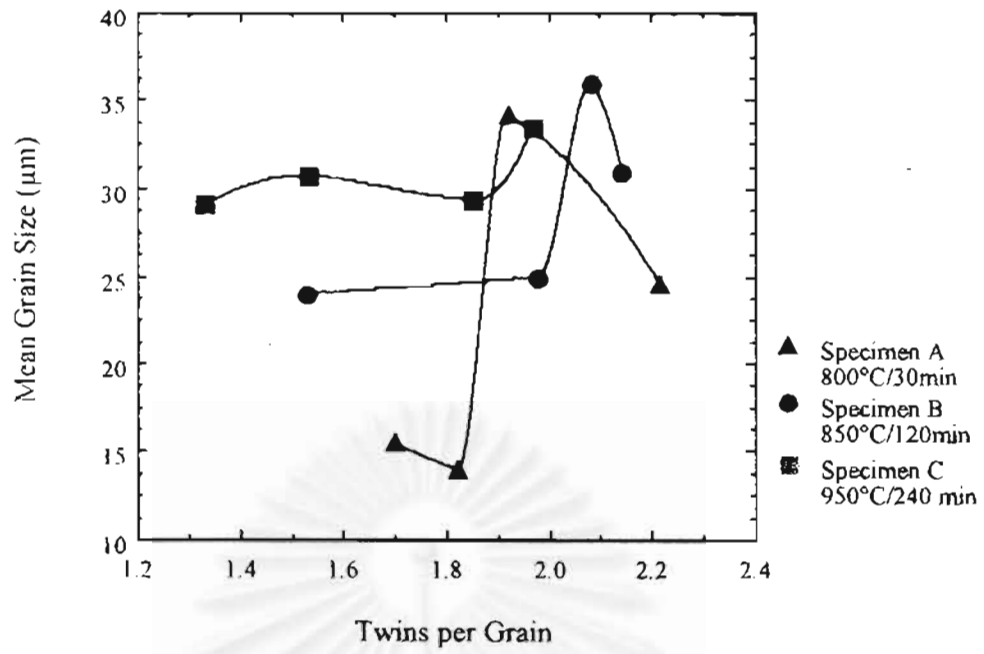
Figure 5.10 Plot of the correlation between twin per grain and grain size
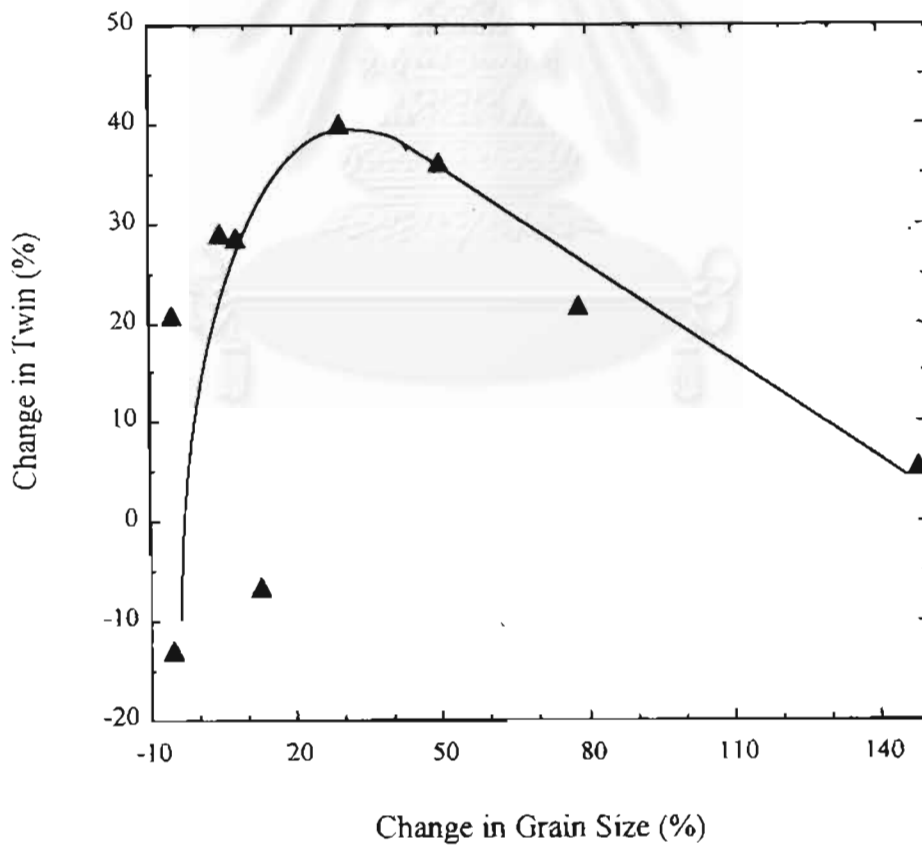
Figure 5.11 Plot showing the change of twin density and change of grain size

The destruction of newly annealing twin is negligible during recrystallization, but is the dominant process during grain growth. As grains begin to grow in low stacking-fault energy, twinning is viewed to occur in order to keep the overall interfacial energy low and thus the increase in twin density is resulted. However, the diving force to reduce the overall interfacial energy by twinning is quickly suppressed by the rate of grain annihilation. Thus, further grain growth results in the decrease in twin density.

By investigation the CSL fraction it was found hat the one-step strain annealing treatment does not significantly affect the CSL distribution, figure 5.12
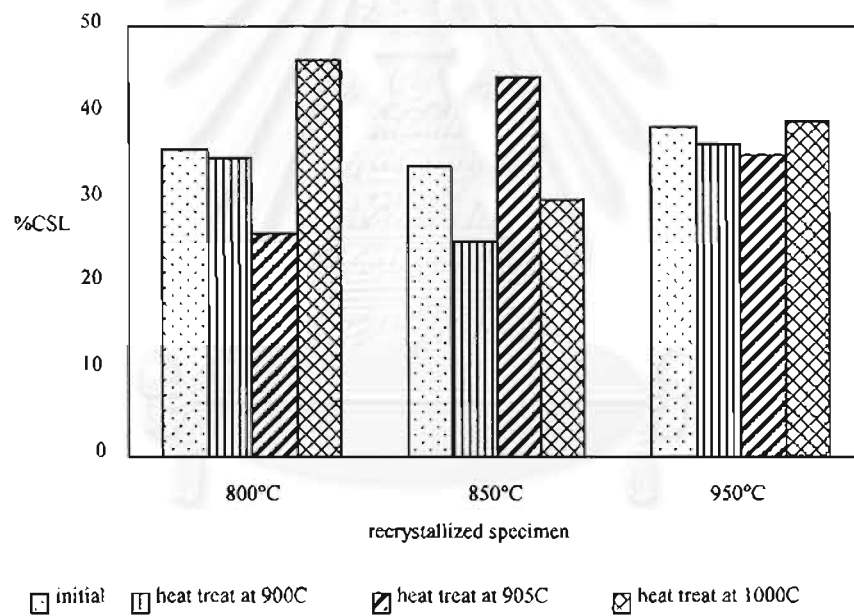
Figure 5.12 The correlation between stain annealing and percent CSL.

Investigation by Schwartz and king [22] on 99.99% oxygen free copper, they succeeded in achieving >70% CSL by performing one-step annealing treatment. However, a big difference may be noted is the impurities presence in our material. Palumbo and Aust [23] study on the effect of impurity in high purity nickel, they pointed

out that the cumulative frequency of low Σ CSL boundaries (i.e., $\Sigma5$ to $\Sigma25$) was found to be strongly dependent on bulk sulphur concentration, with a maximum value of 28% determined for nickel containing 3 ppm S. Nickel grades containing 0.3 ppm S and 10 ppm S were determined to have low Σ (i.e., $\Sigma5$ - $\Sigma25$) frequencies of 17% and 21%, respectively. Frequencies for CSL's in the range (i.e., $\Sigma5$ - $\Sigma25$) were found to be higher than that expected in random distribution (i.e., ~9%). The cumulative frequency at high Σ CSL's (i.e., $\Sigma27$ - $\Sigma49$) was determined to (1) not be strongly influenced by bulk sulphur concentration and (2) be consistent with that expected in a random distribution (i.e., ~5%). The fraction at low angle boundaries ($\Sigma1$) in the distributions was found to vary with sulphur concentration in a manner similar to that noted with the low Σ CSL's (i.e., Σ 5-$\Sigma25$). A maximum frequency of 4.49% was determined with the 3 ppm S grade, and frequencies of 0.96% and 3.5% were determined for the 0.3 ppm S and 10 ppm S grades, respectively.

5.2.3 Iterative strain annealing

In this thesis, the range of recrystallization and strain annealing treatment investigate do not effectively increase the CSL fraction.

Other possible methods [5] to increase the CSL fraction are iterative recrystallization and iterative strain annealing. A concern over the thickness of specimen in the study eliminate the consideration to perform heavily cold work, and then iterative strain annealing was pursued. Was et al. [24] performed in alloy 600 (Ni-16Cr-9Fe) defromation of 2-5% followed by anneals at 890-940°C for1-20h have been found to increase the proportion of Σ3s and Σ9s from 6 to 12% and 5 to 12%, respectively.

In this study, specimens strain annealed at 950°C was further repeated twice and metallographic observations and CSL fraction were measured during each step. Table 5.7 summary results of iterative strain annealing.
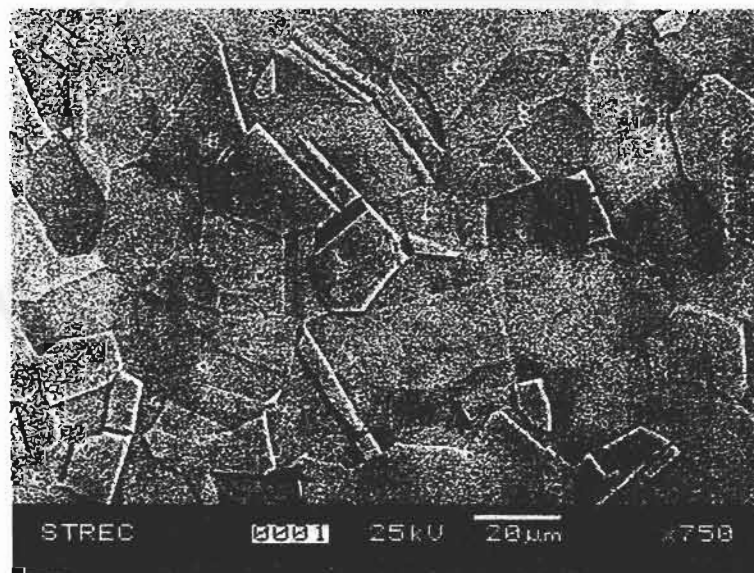
Figure 5.13 The microstructure of iterative strain annealed of 304 stainless steel.

Table 5.7 Summary of iterative strain annealed results.

Sample	Percent CSL	Percent LAB	Percent Σ 3	Grain size (µ)m
950°c_10 min				
800°c	25.53	6.01	24.02	24.6
850°c	44.21	2.88	41.22	31.1
950°c	39.04	3.86	35.53	28.2
950°c_10 min-2				
800°c	40.99	5.94	35.06	28.8
850°c	28.06	4.59	22.99	31.6
950°c	38.82	3.14	30.55	30.5
950°c_10 min-3				
800°c	45.30	3.86	39.80	31.3
850°c	53.91	3.64	49.66	29.6
950°c	46.41	0.83	41.56	27.5
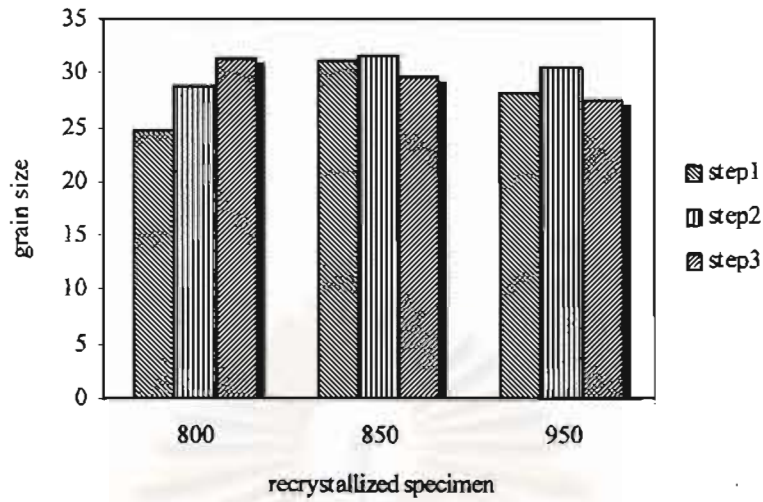
Figure 5.14 The grain size in each step of iterative strain annealed.

Figure 5.14 show that the grain size in each step is not significantly changed in all step of this process.
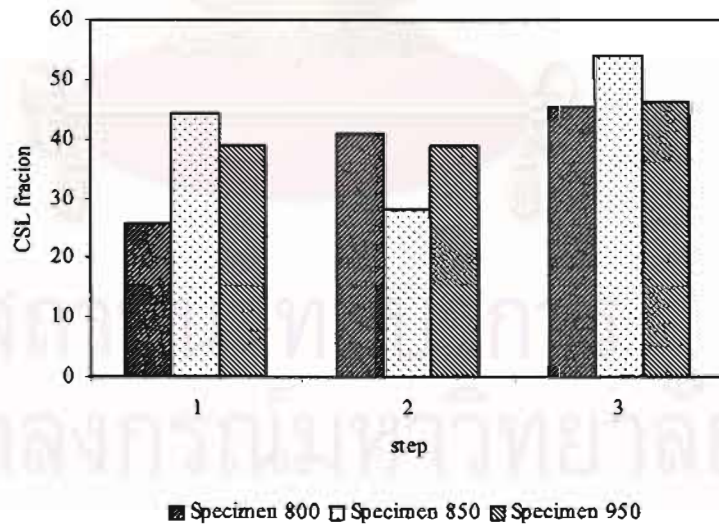
Figure 5.15 The correlation between percent CSL and annealing temperature.

The results of the amount of CSL fraction after each heat-treating steps show that the CSL fraction is highest in the specimen recrystallized at 850°C iteratively annealed at 950°C 10 min three times.

Overall the CSL fraction after the third treatment slightly increased. The maximum CSL fraction observed contains 54% CSL. According to the figure 5.15 the CSL fraction of 54% should result in a reduction of maximum intergranular crack length by 2.5 times compound to 35% CSL, Figure 5.16 shows the extrapolation of the effect of CSL on crack length. To evaluate the effect of CSL on intergranular corrosion of 304 stainless steel, 2 specimens of different CSL fraction were selected for sensitization study. These specimens were heat treated at 650°C for 2h aimed to cause the chromium depletion at grain boundaries due to formation of Chromium carbide. The sensitized specimen ecthed with oxalic acid will attack grain boundary with low chromium carbide. Figure 5.17, 5.18 show the specimens which had CSL fraction 54% and 36% after sensitized at 650°c for 2 hr.
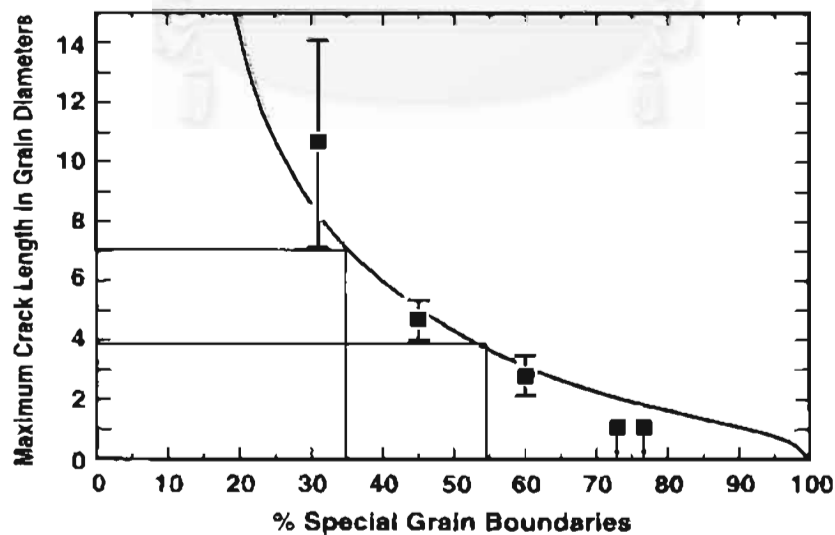
Figure 5.16 The extrapolation of the effect of CSL on crack length [20].

It can be concluded that an increasing CSL fraction from 36% to 54% significantly improve intergranular property of 304 stainless steel.
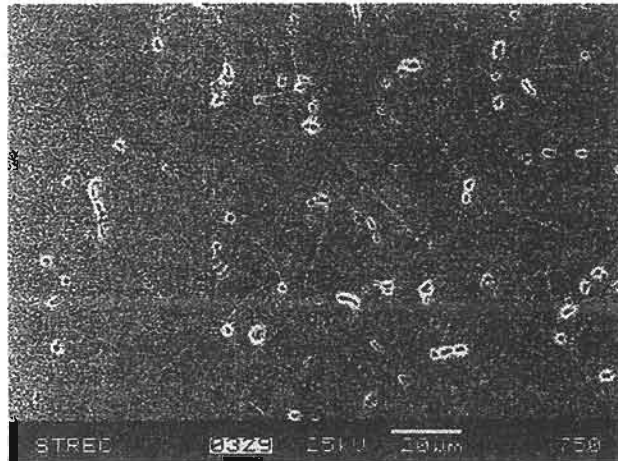
Figure 5.6 The 0.54% CSL fraction specimen after sensitized 650°C/2hr.
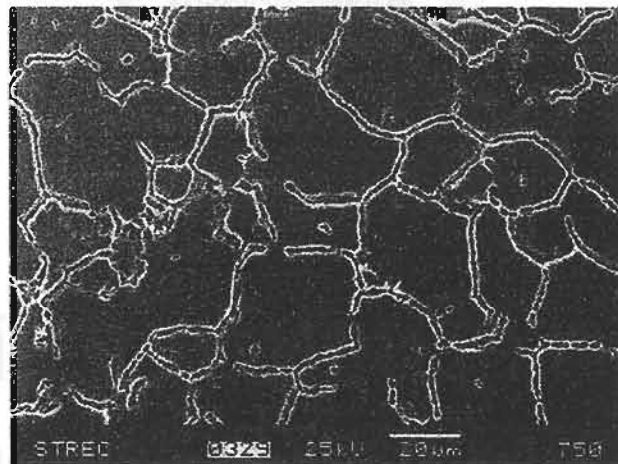
Figure 5.7 The 0.36 CSL fraction specimen after sensitized 650°C/2hr.

Conclusion

The method to improve the intergranular properties of 304 stainless steel by increasing the CSL boundary population can be done by thermomechanical process. The one step strain recrystallization and strain annealing can not adequately increase the population of CSL to resistant to intergranular cracking while the iterative strain annealing can increase the CSL population up to 54%. In this our test the recrystallized specimen at 850 °C which preformed the iterative strain annealing for 3% reduction in thickness and heat treated at 950°C for 3 times can be the effective process to increase the CSL population. There are a little different on the 54% CSL specimen and 36% CSL specimen but after sensitized both specimens, the result shown that there are a great different in the intergarular cracking resistance.

References

1. M. G. Fontana. <u>Corrosion Engineering</u>. 3rd ed. Singapore : McGraw-Hill inc, 1987.

2 O. Wachter and G. Brümmer. "Experienced with Austenitic Steels in Boiling Water Reactors," <u>Nuclear engineering and Design</u> 168(1997) : 35-52.

3 V. Thaveepringsriporn, A. Junyuyen and W. Ratanachai. "On the Relation Between Grain Boundary Misorientation and Intergranular Carbides in Stainless Steels Using Selected Area Channeling Patterns," <u>Journal of Electron Microscopy society of Thailand</u> 11(1996) : 24-29.

4 P. Lin, G. Palumbo and K.T, Aust. "Experimental Assessment of the Contribution of Annealing Twins to CSL Distributions in FCC Materials, <u>Scripta materialia</u> 36 (1997) :1145-1149.

5 V. Randle, "Mechanism of Twinning-Induced Grain Boundary Engineering in Low Stacking-Fault Energy Materials," <u>Acta mater</u> 47(1999) : 4187-4196.

6 J. Mizera and J.W. Wyrzkowski. "An Analysis of the Twin Boundaries on Mechanical Properties of Austinetic Steel," <u>Materials Science and Engineering</u> A112(1989) : 39-42.

7 R. A. Varin and J. Kruszynska "Control of Annealing Twins in Type 316 Austenitic Stainless Steel," <u>Acta Metall</u> 35(1987) : 1767-1774.

8 E.M. Lehockey, G. Palumbo and A.M. Brennentuhl. "On the Relationship between Grain Boundary Character Distribution and Intergranular Corrosion," <u>Scripta Materiialia</u> 36(1997) : 1211-1218.

References (cont.)

9   M. A. Meyer and C. McCowan. The Formation of Annealing Twins: Overview and New Thoughts," The Center for Explosives Technology Research. (unpublished research).

10 C. S Pande, M. A. Iman and B. B. Rath. "Annealing Twins in f.c.c Metals and Alloy," Naval research Laboratory. (unpublished research).

11 R. L. Fullman and J. C. Fisher. " Formation of Annealing Twins During Grain Growth," Journal Applied Physics 22(1951) : 1350-1355.

12 G. Gindraux and W. Form " New Concepts of Annealing-Twin Formation in Face-Centred Cubic Metals," Journal of Institute of Metals 101(1973) : 85-93.

13 W. Form, G. Gindraux and V. Miyncar. "Density of Annealing Twins," Metal Science 14(1980) : 16-20.

14 V. Randle' "Microstructure Investigation of Relationship Between Strain and Anomalous Grain Growth," Philosophical Magazine A 67(1993) : 1301-1313.

15 M. Schweizer and W. Form. Ibid 101(1973):85, cited in W. Form, G. Gindraux and V. Miyncar. Metal Science 14(1980) : 16-20.

16 V.Y. Gertsman, M. Janecek and K. Tangri. "Grain Boundary Ensembles in Polycrystals," Acta Matter 44(1996) : 2869-2882.

17 V. Randle. Microtexture Determination and its Application. The Institute of Materials, 1992.

18 www. noran.com.

19 V. Randle. The Measurement of Grain Boundary Geometry. Institute of Physics Publishing, 1993.

References (cont.)

20 G. Palumbo, E.M. Lehockeyy and P. Lin. "Applications for Grain Boundary Engineering Materials," JOM 50(1998) : 40-43.

21 K.J. Kurzydlowski. "Grain Geometry Evolution in the Process of Grain Growth Induced by Temperature and Plastic Deformation-Problem of the Incubation period," Scripta METALLURGICA et MATERIALIA 27(1992) : 871-874.

22 A.J. Schwartz and W.E. King. "The Potential Engineering of Grain Boundaries through Thermomechanical Processing," JOM 50(1998) : 50-55.

23 G. Palumbo and K.T. Aust. "Grain Boundary Character Distributions in Nickel," The Minerals, Metals & Materials Society. (1990) : 101-111.

24 G.S. Was, V. Thaveeprungsriporn and D.C. Crawford. "Grain Boundary Misorientation Effect on Creep and Cracking in Ni-based Alloys," JOM 50 (1998) :44-49.

APPENDIX

APPENDIX

ELECTRON BEACK-SCATTERING DIFFRACTION DATA

Specimen condition: *1050°C/2hr + 30% reduction in thickness + 800°C/30 min specimen.*

Grain Boundary type	First run	Second run
$\Sigma 3$	0.91	0.8876
$\Sigma 5$	0.0063	0.0139
$\Sigma 7$	0.0148	0.0143
$\Sigma 9$	0.0224	0.0745
$\Sigma 11$	0.0164	0.0016
$\Sigma 13$	-	0.0079
$\Sigma 15$	0.0038	-
$\Sigma 17$	0.0013	-
$\Sigma 19$	0.0047	-
$\Sigma 21$	0.0088	-
$\Sigma 25$	0.0025	-
$\Sigma 27$	0.0076	-
$\Sigma 29$	0.0013	-
Number of grain measurement	209	186

Specimen condition: *1050°C/2hr + 30% reduction in thickness + 850°C/2hr specimen.*

Grain Boundary type	First run	Second run
Σ3	0.9404	0.9267
Σ5	0.0288	0.0133
Σ7	0.0019	0.0133
Σ9	0.0096	0.0213
Σ11	0.0154	0.0129
Σ13	0.0019	0.0125
Σ15	0.0019	-
Number grain of measurement	108	193

Specimen condition: *1050°C/2hr + 30% reduction in thickness + 950°C/4hr specimen.*

Grain Boundary type	First run	Second run
Σ3	0.8812	0.9341
Σ5	0.0086	0.0096
Σ7	0.0120	0.0157
Σ9	0.0763	0.0365
Σ11	0.0206	-
Σ13	0.0012	0.0043
Σ15	-	-
Number grain of measurement	100	87

Specimen condition: *1050°C/2hr + 30% reduction in thickness + 800°C/30 min*

specimen + 3% reduction in thickness +900°C/10 min

Grain Boundary type	First run	Second run
Σ3	0.7978	0.8485
Σ5	0.0103	0.0027
Σ7	0.0082	0.0214
Σ9	0.1003	0.0695
Σ11	0.0164	0.0398
Σ13	0.0311	0.0100
Σ15	-	0.0080
Σ17	0.0148	-
Σ19	0.0124	-
Σ21	0.0021	-
Σ25	0.0042	-
Σ27	0.0021	-
Number of grain measurement	101	112

Specimen condition: *1050°C/2hr + 30% reduction in thickness + 800°C/30 min*

specimen + 3% reduction in thickness +950°C/10 min

Grain Boundary type	First run	Second run
Σ3	0.8981	0.9597
Σ5	0.0140	-
Σ7	-	0.0101
Σ9	0. 506	0.0202
Σ11	0.0140	-
Σ13	0.0140	0.0101
Σ15	0.0093	
Number of grain measurement	68	53

Specimen condition: *1050°C/2hr + 30% reduction in thickness + 800°C/30 min*

specimen + 3% reduction in thickness +1000°C/10 min

Grain Boundary type	First run	Second run
Σ3	0.8858	0.9480
Σ5	-	0.0094
Σ7	0.0154	-
Σ9	0.0856	0.282
Σ11	0.0022	0.0071
Σ13	-	0.0047
Σ21	0.0044	-
Σ23	0.0066	0.0024
Number of grain measurement	54	56

Specimen condition: *1050°C/2hr + 30% reduction in thickness + 850°C/2hr specimen +*

3% reduction in thickness +900°C/10 min

Grain Boundary type	First run	Second run
Σ3	0.7597	0.8323
Σ5	0.325	0.0255
Σ7	0.0098	-
Σ9	0.1232	0.0666
Σ11	0.0358	0.0444
Σ13	0.0390	0.0311
Number of grain measurement	110	96

Specimen condition: *1050°C/2hr + 30% reduction in thickness + 850°C/2hr specimen +*

3% reduction in thickness +950°C/10 min

Grain Boundary type	First run	Second run
Σ3	0.9015	0.9535
Σ5	0.0148	0.0255
Σ7	0.0185	0.0142
Σ9	0.0430	0.0044
Σ11	0.0148	-
Σ13	0.0074	-
Σ19	-	0.0024
Number of grain measurement	52	61

Specimen condition: *1050°C/2hr + 30% reduction in thickness + 850°C/2hr specimen +*

3% reduction in thickness +950°C/10 min

Grain Boundary type	First run	Second run
$\Sigma 3$		
$\Sigma 5$		
$\Sigma 7$		
$\Sigma 9$		
$\Sigma 11$		
$\Sigma 27$		
$\Sigma 29$		
Number of grain measurement		

.

Specimen condition: *1050°C/2hr + 30% reduction in thickness + 850°C/2hr specimen +*

3% reduction in thickness +1000°C/10 min

Grain Boundary type	First run	Second run
$\Sigma 3$	0.9030	0.8376
$\Sigma 5$	0.0397	0.0466
$\Sigma 7$	-	0.0138
$\Sigma 9$	0.0441	0.0798
$\Sigma 11$	0.0044	0.0166
$\Sigma 13$	0.0088	0.0028
Number of grain measurement	59	88

Specimen condition: *1050°C/2hr + 30% reduction in thickness + 950°C/4hr specimen +*

3% reduction in thickness +900°C/10 min

Grain Boundary type	First run	Second run
Σ3	0.8912	0.8598
Σ5	0.0240	-
Σ7	-	0.0105
Σ9	0.0240	0.0382
Σ11	0.0160	0.0526
Σ13	0.0196	-
Σ17	-	0.0363
Σ23	-	0.0026
Number of grain measurement	92	60

Specimen condition: *1050°C/2hr + 30% reduction in thickness + 950°C/4hr specimen +*

3% reduction in thickness +950°C/10 min

Grain Boundary type	First run	Second run
Σ3	0.8154	0.9287
Σ5	0.0682	0.0082
Σ7	0.0131	0.0509
Σ9	0.0710	0.0082
Σ11	0.0094	-
Σ13	0.0065	0.0041
Σ15	0.0163	-
Number of grain measurement	62	44

Specimen condition: *1050°C/2hr + 30% reduction in thickness + 950°C/4hr specimen +*

3% reduction in thickness +1000°C/10 min

Grain Boundary type	First run	Second run
Σ3	0.8954	0.9219
Σ9	0.0884	0.0677
Σ11	0.0054	0.0083
Σ17	-	0.0021
Σ21	0.0108	-
Number of grain measurement	66	81

Specimen condition: *1050°C/2hr + 30% reduction in thickness + 800°C/30 min*

specimen + 3% reduction in thickness +950°C/10 min + 3%

reduction in thickness +950°C/10 min

Grain Boundary type	First run	Second run
Σ3	0.8320	0.8829
Σ5	0.0018	0.0023
Σ9	0.1213	0.0460
Σ11	0.0108	0.0069
Σ13	0.0018	0.0276
Σ17	0.0072	0.0319
Σ19	0.0216	-
Σ21	-	0.0023
Σ27	0.0036	-
Number of grain measurement	95	93

Specimen condition: *1050°C/2hr + 30% reduction in thickness + 850°C/2hr specimen + 3% reduction in thickness +950°C/10 min + 3% reduction in thickness +950°C/10 min*

Grain Boundary type	First run	Second run
Σ3	0.8891	0.7420
Σ5	0.0325	0.0029
Σ7	0.0240	0.0460
Σ9	0.0190	0.0958
Σ11	0.0162	0.0883
Σ13	0.0190	0.0166
Σ17	-	0.0332
Σ19	-	0.0033
Σ21	-	0.0100
Σ27	-	0.0033
Number of grain measurement	118	130

Specimen condition: *1050°C/2hr + 30% reduction in thickness + 950°C/4hr specimen +*

3% reduction in thickness +950°C/10 min + 3% reduction in

thickness +950°C/10 min

Grain Boundary type	First run	Second run
$\Sigma 3$	0.8232	0.7419
$\Sigma 5$	0.0249	0.0268
$\Sigma 7$	0.0161	0.0190
$\Sigma 9$	0.1175	0.1472
$\Sigma 11$	0.0092	0.0570
$\Sigma 13$	-	0.0136
$\Sigma 15$	-	0.0027
$\Sigma 17$	0.0023	-
$\Sigma 27$	0.0069	-
Number of grain measurement	84	101

Specimen condition: *1050°C/2hr + 30% reduction in thickness + 800°C/30 min specimen + 3% reduction in thickness +950°C/10 min + 3% reduction in thickness +950°C/10 min + 3% reduction in thickness +950°C/10 min.*

Grain Boundary type	First run	Second run
$\Sigma 3$	0.8895	0.8696
$\Sigma 5$	0.0024	0.0039
$\Sigma 7$	0.0048	-
$\Sigma 9$	0.0891	0.1105
$\Sigma 11$	0.0024	0.0056
$\Sigma 15$	-	0.0064
$\Sigma 17$	-	0.0039
$\Sigma 21$	0.0024	-
$\Sigma 25$	0.0024	-
$\Sigma 27$	0.0071	-
Number of grain measurement	75	86

Specimen condition: *1050°C/2hr + 30% reduction in thickness + 850°C/2hr specimen + 3% reduction in thickness +950°C/10 min + 3% reduction in thickness +950°C/10 min + 3% reduction in thickness +950°C/10 min.*

Grain Boundary type	First run	Second run
$\Sigma 3$	0.9019	0.9429
$\Sigma 5$	0.0384	-
$\Sigma 7$	0.0107	0.0114
$\Sigma 9$	0.0472	0.0457
$\Sigma 19$	0.0018	-
Number of grain measurement	67	47

Specimen condition: *1050°C/2hr + 30% reduction in thickness + 950°C/4hr specimen +*
3% reduction in thickness +950°C/10 min + 3% reduction in
thickness +950°C/10 min + 3% reduction in thickness +950°C/10
min.

Grain Boundary type	First run	Second run
Σ3	0.9331	0.8577
Σ5	-	0.0145
Σ7	-	0.0287
Σ9	0.0607	0.0411
Σ11	0.0020	0.0310
Σ13	0.0041	0.0062
Σ17	-	0.0166
Σ25	-	0.0021
Σ27	-	0.0021
Number of grain measurement	71	77

Biography

Miss Piyaporn Sinsrok was born on January 27, 1973 at Amphur Muang, Nakornrachasima province. After granted the Bachelor degree of Science at Kasetsart University. In 1996 started to study in program Master Degree of Science, in Nuclear Technology Department, Faculty of Engineering, Chulalongkorn University.